



HAL
open science

Neogene to ongoing normal faulting in the inner western Alps: A major evolution of the late alpine tectonics.

Christian Sue, Pierre Tricart

► To cite this version:

Christian Sue, Pierre Tricart. Neogene to ongoing normal faulting in the inner western Alps: A major evolution of the late alpine tectonics.. *Tectonics*, 2003, 22, pp.1050. 10.1029/2002TC001426 . hal-00103817

HAL Id: hal-00103817

<https://hal.science/hal-00103817>

Submitted on 10 Feb 2021

HAL is a multi-disciplinary open access archive for the deposit and dissemination of scientific research documents, whether they are published or not. The documents may come from teaching and research institutions in France or abroad, or from public or private research centers.

L'archive ouverte pluridisciplinaire **HAL**, est destinée au dépôt et à la diffusion de documents scientifiques de niveau recherche, publiés ou non, émanant des établissements d'enseignement et de recherche français ou étrangers, des laboratoires publics ou privés.

Neogene to ongoing normal faulting in the inner western Alps: A major evolution of the late alpine tectonics

Christian Sue

Institut de Géologie, Université de Neuchâtel, Neuchâtel, Switzerland

Pierre Tricart

Laboratoire de Géodynamique des Chaînes Alpines, Observatoire des Sciences de l'Univers de Grenoble, Grenoble, France

Received 6 June 2002; revised 28 November 2002; accepted 28 January 2003; published 3 October 2003.

[1] Widespread brittle extension occurs in the internal zones of the southwestern Alps, forming a dense fault network, which overprints the compressional structures. The extension has been followed by transcurrent motions. In terms of paleostress this extension is radial to the belt close to the Crustal Penninic Front and multidirectional in the eastern part of the internal zones. The paleostress field of the strike-slip phase is coherent with the extensional one and compatible with dextral shear along longitudinal faults. Globally, we propose that the internal zones of the southwestern Alps underwent a single Neogene transtensive tectonic regime. To strengthen our structural results, the current tectonics has been analyzed using seismotectonic tools. This approach allowed the recognition of several active faults. Moreover, the ongoing tectonics is coherent with the observed brittle deformation. The fault network controls the present-day seismicity. The combined seismotectonic and structural approaches give coherency and continuity from the Neogene to ongoing extensional tectonics in the southwestern Alps. In the framework of the whole western Alps a synthesis of our results with neotectonic-related data allowed us to provide an accurate map of the Neogene to present kinematics of the belt. Extension, which appears as a major feature of the internal zones, has been coeval with the propagation of thrusts in the outer zones during Neogene times. The geodynamic processes, which rule this major tectonic evolution of the belt, remain a matter of debate.

INDEX TERMS: 7230 Seismology: Seismicity and seismotectonics; 8010 Structural Geology: Fractures and faults; 8102 Tectonophysics: Continental contractional orogenic belts; 8107 Tectonophysics: Continental neotectonics; 8164 Tectonophysics: Stresses—crust and lithosphere; **KEYWORDS:** western Alps, normal faulting, neotectonics, Neogene tectonics, active faulting. **Citation:** Sue, C., and P. Tricart Neogene to ongoing normal faulting in the inner western Alps: A major

evolution of the late alpine tectonics, *Tectonics*, 22(5), 1050, doi:10.1029/2002TC001426, 2003.

1. Introduction

[2] The western Alps result from the subduction of the Tethyan Ocean and the subsequent collision between European and African margins since the Late Cretaceous [e.g., *Trumphy*, 1960; *Lemoine et al.*, 1986; *Dewey et al.*, 1989; *Laubscher*, 1991; *Schmid and Kissling*, 2000]. Main emphasis has long been placed on the detailed nappe structure and the compressional nature of the chain. The stacked nappes built a sedimentary, a crustal, and a lithospheric collision prism [*Nicolas et al.*, 1990], arc-shaped around the western edge of the Adria indenter, an African northern promontory [*Argand*, 1924; *Pavoni*, 1961; *Tapponnier*, 1977; *Channel et al.*, 1979]. Nevertheless, seismotectonic analyses have recently shown that the current activity of the western Alps is dominated by radial extension in their internal zones [*Sue et al.*, 1999]. We focus here on the South Pelvoux segment, a key area of the southwestern alpine arc (French-Italian Alps, Figure 1 [*Kerckhove et al.*, 1979]), characterized by the contrast of the external and the internal arcs [*Tricart*, 1984; *Tricart and Lemoine*, 1986; *Frey et al.*, 1999]. This paper deals with the late alpine tectonics in the internal arc to the present-day tectonic regime. The aim is to link the ongoing active extension to the late alpine brittle deformation.

2. Geological and Tectonic Setting

[3] In the South Pelvoux area (Figure 1) the internal alpine arc consists of a pile of high-pressure/low-temperature metamorphic thrust sheets involving the basement and its sedimentary cover. Deformation and metamorphism increase toward the east across the Briançonnais and Piémont zones. The Piémont zone originated as an accretionary prism linked to the Late Cretaceous-early Tertiary subduction of the Tethys and of the lower European continental margin. During the Eocene collision the prism grew westward to involve the middle part of the margin. This formed the Briançonnais zone. The internal arc basically originates from this Paleogene, mainly Eocene, accretionary prism. Along its western front, in the external domain (old upper European continental margin), a flexural basin developed with turbidites deposited in early Oligocene times (Champ-

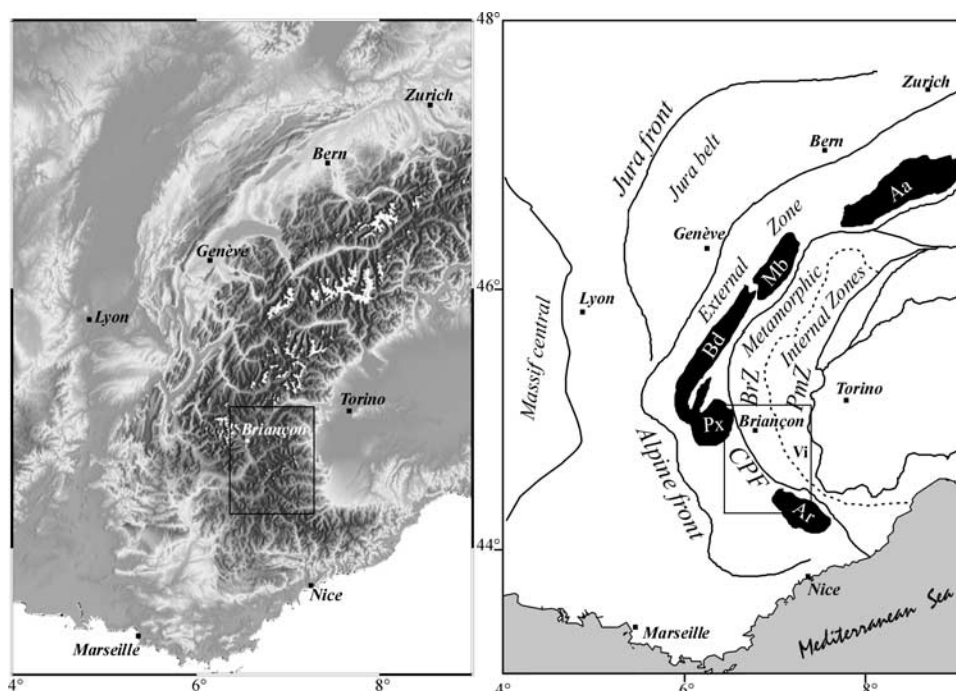


Figure 1. DEM and tectonic sketch map of the western Alps between France, Switzerland, and Italy. We focus in this paper on late alpine to present tectonics of the internal zones, made of the Briançonnais zone (BrZ) and Piémontais zone (PmZ). The study area (frame) is located around and south of the Briançon region, between the Pelvoux (Px), Viso (Vi) and Argentera (Ar) massifs. The external crystalline massifs in black follow the arcuate geometry of the belt (Aa, Aar; Mb, Mont Blanc; Bd, Belledonne). CPF is the Oligocene “Crustal Penninic Front”, by now reactivated as a crustal detachment.

saar Sandstones, Annot Sandstones) due to the major westward thrusting of the internal zones onto the external domain along the Crustal Penninic Front (CPF). To the north, along the deep seismic profile ECORS, this thrust surface was interpreted as a lithospheric ramp, along which the offset of the Moho would approach 80 km [Mugnier *et al.*, 1993].

[4] In the footwall of this Oligocene thrust, west verging folds and thrusts formed to the external arc characterized by radial directions of transport [Gratier *et al.*, 1989; Vialon *et al.*, 1989]. Thin-skinned and basement-involved tectonics corresponds to a general shortening that remains much lower than in the internal arc and inversion tectonic style (reactivation of former normal faults) still prevails in many places [de Graciansky *et al.*, 1989]. Shortening phases accentuated during the Miocene [Tricart, 1984; Coward *et al.*, 1989], building the external arc that would remain active today. Their effect was to push away the alpine front beyond the limits of the old extended Tethyan margin [Lemoine *et al.*, 1986] and to uplift the basement in the external crystalline massifs as shown by fission track analyses [Seward and Manktelow, 1994; Fügenschuh *et al.*, 1999]. This uplift still remains active, as established by leveling data [Levallois, 1972; Schaer and Jeanrichard, 1974; Fourniguet, 1977; Ménard, 1988].

[5] Up to now, the coeval evolution in the internal arc was thought to be dominated by the general shortening,

generating east directed late structures (back thrusting/folding). These are the Briançonnais backfolds and Piémont backthrusts that constitute the eastern branch of the alpine fan-shaped structure [e.g., Tricart, 1984]. This scenario began to be questioned when ductile normal faults and extensional detachments were discovered in the Piémont zone [Ballèvre *et al.*, 1990; Philippot, 1990; Black and Jayko, 1990]. Late alpine normal faults were then locally described in the Piémont zone [Lazarre *et al.*, 1994] and Briançonnais zone [Virlovvet *et al.*, 1996]. They actually correspond to widespread structures that have now been systematically analyzed in the whole area between Pelvoux, Argentera, and Viso massifs [Sue, 1998].

[6] In the target region, late alpine normal faulting is limited by the Penninic front; that is, it is restricted to the internal arc. Locally, Sue and Tricart [1999] demonstrated that the inversion of this major thrust as an extensional detachment is connected with a brittle extension in its hanging wall, itself connected to the regional-scale extension in the internal arc. Recent preliminary thermochronological data (fission tracks) indicate that the inversion of the Penninic Frontal Thrust and the brittle extension in its hanging wall in the target area (Briançon region) began in the latest Oligocene and went on during the Miocene [Tricart *et al.*, 2001]. Fission track analyses also indicate similar results in the northwestern Alps [Seward and Manktelow, 1994; Fügenschuh *et al.*, 1999]. Finally, it was recently

demonstrated that the seismicity in the internal arc corresponds to an extensional tectonics [Sue *et al.*, 1999]. On the whole, the classic scenario was not addressing recent tectonics, as the internal arc's tectonics was dominated during the Neogene by extension, when the external arc essentially suffered westward propagation of the alpine compressive front and a general accentuation of the fold-thrust structure. In the following, we analyze this widespread Neogene normal faulting in the internal zones along the South Pelvoux segment, we constrain the corresponding stress/strain field, and we demonstrate that this brittle extension controls the present-day seismotectonic regime.

[7] Two main tectonic ensembles have been analyzed:

[8] 1. The Briançonnais sedimentary cover thrust sheets are along the Durance and High Ubaye valleys [Barf  ty *et al.*, 1996; Debelmas and Lemoine, 1966; Gidon *et al.*, 1994] (for stratigraphic details, see Claudel and Dumont [1999]). The main structure is a pile of small nappes, detached along the Triassic evaporites, of Middle/Late Triassic dolomite-rich platform carbonates forming a rigid sole (anterior). Basal nappes are detached at the top of a thick carboniferous coal-rich series, the rigid sole being made of 300 m of Permian conglomerates and Early Triassic quartzites. Overlying Liassic to Dogger shales, marls, and limestones (synrift) display a contrasted tectonic behavior. The postrift sequence is made of Middle-Late Jurassic limestones and marls and shales of Cretaceous/Eocene age forming a homogeneous incompetent ensemble. From west to east the tectonic style evolved from flat-lying superposed slabs to recumbent folds sliced up into subunits in disharmonic folds. The metamorphism associated with these Eocene structures increases eastward from lawsonite bearing greenschist to low-grade blueschist facies. Oligocene superimposed structures are new recumbent folds associated to west verging thrusts and east verging long-wavelength folds. This folded pile of nappes behaves as a highly contrasted multilayer structure.

[9] 2. The Pi  mont Schistes lustr  s complex lies between the Briançonnais nappes and the Monviso ophiolite (Chenaillat massif, Queyras, High Ubaye valley). The Schistes lustr  s derive mainly from deep-sea marl-rich sediments deposited in the Tethyan ocean or on the distal European passive margin. They are highly foliated caleschists containing some boudins of ophiolites and Triassic dolomites [Tricart and Lemoine, 1986]. Imbricated thrust sheets built a plurikilometric accretionary wedge that underwent at least three phases of isoclinal folding mainly during the Paleogene. The associated metamorphism evolves through time from blueschist to greenschist conditions. With respect to the late faulting, the general structure behaves as a unique huge volume of not very competent but highly anisotropic material. Some marker levels (e.g., Tithonian marbles) allow the regional geometry to be partly understood [Lemoine and Tricart, 1993]. The last phase of ductile deformation corresponds to a regional-scale extension. The ductile-brittle transition has been analyzed by Schwartz [2002]. As extension went on, ductile to brittle transition occurred during the Miocene, forming the widespread normal faulting analyzed in this paper. Inside the regional

flat-lying cleavage, a multidirectional extension developed, characterized by chocolate tablet boudinage. On these ductile extensional structures, conjugated micronormal faults merged subsequently. Their directions also characterize an oblate strain ellipsoid. At the same period the regional structure is tilted westward, in the western flank of the Dora-Maira massif. Fission track analyses show that this differential exhumation took place during the Miocene [Schwartz *et al.*, 2003]. Then, larger normal faults developed under brittle conditions. These last ones correspond to the late evolution that we analyze here.

3. Brittle Deformation Analysis

[10] The studied area is carved by a dense fault network, which corresponds to the last tectonic event in the alpine history. Indeed, this fault network postdates all the alpine compression-related structures such as nappe piles, folds, and schistosity and cleavages related to the different compressional phases. The late fault system is made of normal faults, which locally bear witness of transcurrent reactivation. They can be observed at every scale (kilometric to centimetric) in the field. Some of the major faults have already been described as wrench faults (e.g., the Durance fault, see discussion by Tricart *et al.* [1996]), although they are generally not shown on geological maps.

3.1. Late Alpine Fault Network: Regional-Scale Analysis

[11] We first mapped the fault network in detail. To achieve this map, we used field work, aerial photographs, remote sensing and digital elevation model (DEM) analyses. These analyses were possible due to interactions and feedback between the field and remote sensing work sessions. The larger-scale analysis is provided by the SPOT satellite view of the Brian  on region. A couple of SPOT images have been used to compute the DEM of the region with a high spatial accuracy (down to 10 m) (Figures 2 and 3). At the kilometric scale the main tool used was aerial photographs (Figure 4a). The morphotectonic interpretations of these documents closely associated with field work allow the precise mapping of the fault network (Figure 4a), which is integrated in the southwestern alpine tectonic framework on Figure 4b. These large-scale structural analyses allow the accurate mapping of the geometry of the fault network at the scale of the main alpine tectonic units (external zone, internal Brian  onnais and Piemontais zones, external crystalline massifs, Flysch nappes). The first striking characteristic is the double family distribution of the faults (see white arrows on Figure 3). The first fault family strikes longitudinally (subparallel) to the belt arcuate structure, i.e., NNW-SSE to NW-SE from the north to the south of the studied area. The second fault family strikes transverse (radial) to the belt's structures. These two fault families are recognized at every scale: Seen on larger SPOT scale, they are also observable in the field (outcrop scale) and at smaller scale by microtectonic measurements (slickensides on microfault planes, several centimeters wide, see below). Their global

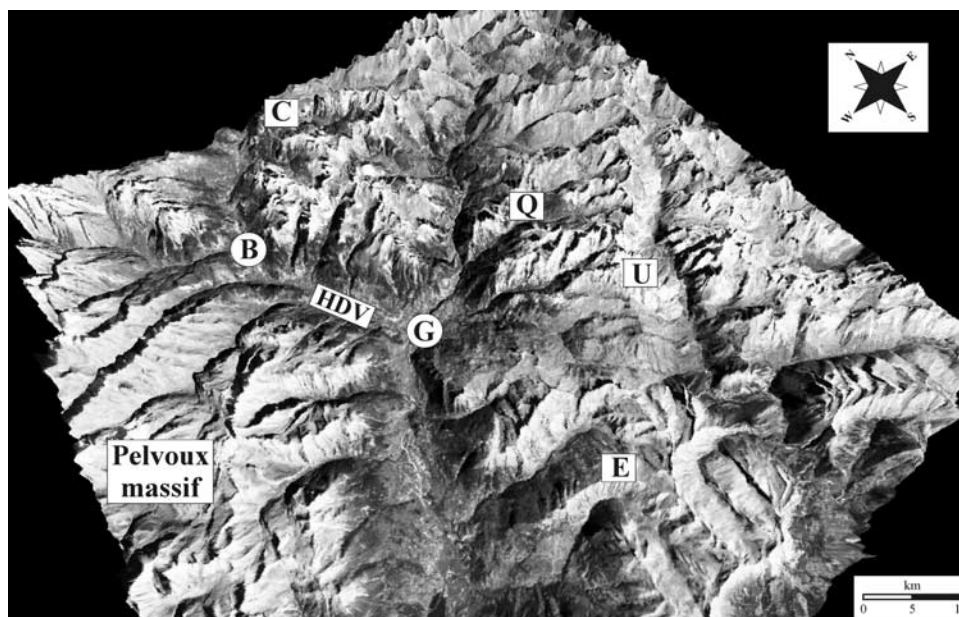


Figure 2. Three-dimensional satellite view toward the northeast of the studied area (SPOT satellite panchromatic orthophotography projected on the DEM). The Briançonnais zone in the vicinity of Briançon (B) and Guillestre (G) towns and in the High Ubaye (U) massif, the adjacent Piémont zone in the Queyras (Q) and Chenaillet (C) massifs, as well as the Embrunais (E) area are carved by a dense late alpine fault network, which rules part of the present-day morphology of the region, particularly along the High Durance valley (HDV).

and local crosscutting relationships show that they developed and worked simultaneously at the regional scale. The longitudinal faults controlled the longitudinal strap-like structure of the Briançonnais zone with numerous close faults (Figure 4). On the contrary, the transverse faults are distributed at pretty large intervals (several kilometers). The main fault family in the Briançonnais zone seems to be the longitudinal one. It is composed of long faults such as the East Briançonnais fault or the Durance-Escreins-Serenne fault, which can be followed along more than 50 km, across the whole studied area, and to the north along the Valloire fault. These two faults localized the longitudinal family into the Briançonnais zone, eastward and parallel to the CPF. One branch associated to the longitudinal fault veers off this direction and strikes N-S across the CPF, in the flysch nappes, to form the Parpaillon fault system. The transverse fault family is also well developed in the Briançonnais as well as in the Piémont zone. It locally crosscuts the CPF and also affects the external zone and the flysch nappes in the Embrunais region. To sum up, the late alpine fault network is made of two fault families, which have worked simultaneously as normal faults under brittle conditions, in response to the same extensional tectonic regime. Later, they have locally been reactivated as transcurrent faults.

3.2. Late Alpine Normal Faulting: Typical Outcrop Analyzes

[12] The overall faulting in this region can be illustrated by some typical outcrops of the Briançonnais nappes showing different kinds of late alpine faults (extensional

faults and strike slips) belonging to both fault families (longitudinal and transverse). In close relationship to the CPF, on the outcrops of the Fournel valley, normal faults are extremely well developed and merge with the CPF at depth. The relationships between the compressional structures of the Briançonnais zone, the CPF, and the late alpine brittle extension are clear in this area [Sue and Tricart, 1999]. The same longitudinal faults occur in the Durance valley, i.e., following the main branch of the High Durance fault zone (Figures 3 and 4). For instance, the Rocher Baron site (Figure 5), south of Briançon in the Durance Valley, shows longitudinal west dipping second-order normal faults (some hundreds of meters) conjugated to the major east dipping High Durance normal fault. The latter is one of the main extensional structures and has a throw >1000 m. This site allows the observation of longitudinal late alpine normal faulting at many scales, from several hundreds of meters down to the centimeter scale. Concerning the transverse fault family, the Melezin site (Figure 6), SE of Briançon, provides a nice example with a large-scale normal fault, postdating the nappe tectonics, a large-scale drag-fold anticline, conjugated microfaults with striae and calcareous fibers, small-scale drag-folds postdating the schistosity, etc. Figures 7 and 8 give an example of extensional structures overprinting compressional structures in the Chambeyron massif (High Ubaye), at mesoscale and nappe scale, respectively. Locally, the normal faults have been reactivated by strike-slip movements. The timing of the normal displacement and the transcurrent one is clear in the polyphased sites (i.e., where both normal and strike-slip motions have been observed; see below for the

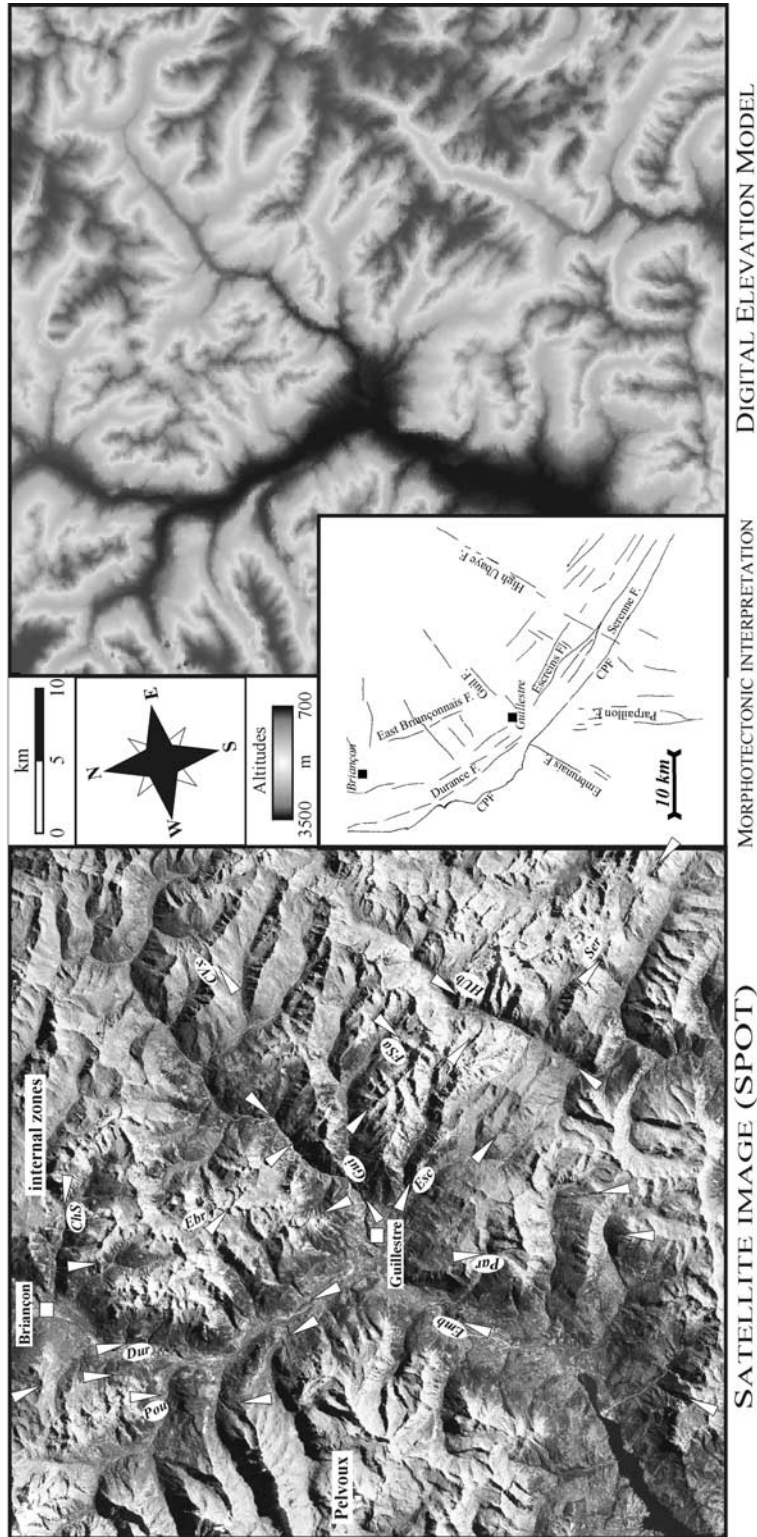
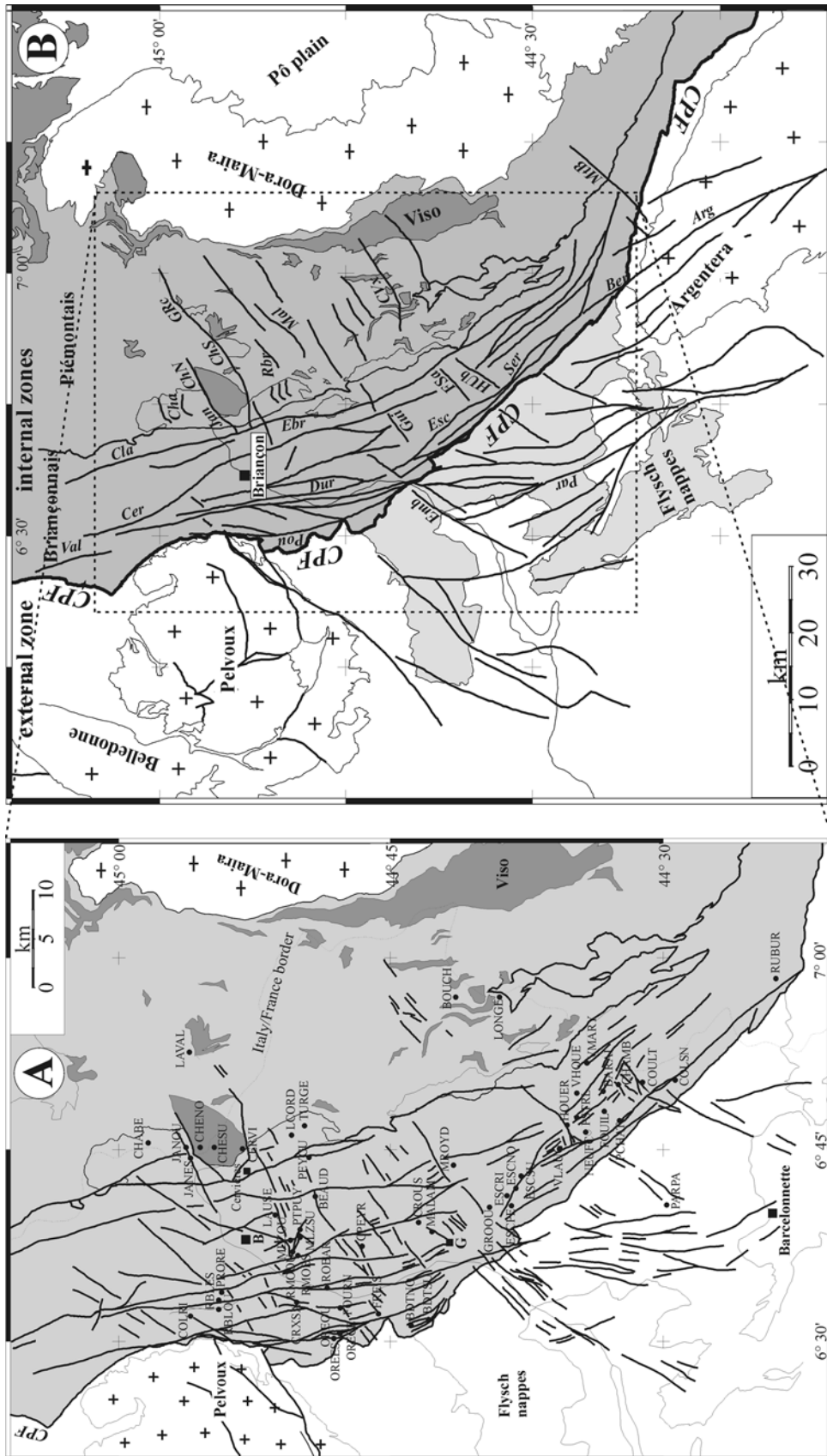


Figure 3. Morphotectonic analysis of the region south of Briançon, combining remote sensing (thin 10 m DEM, and 10 m SPOT satellite image) and field work expertise. These documents allow us to precisely characterize the fault pattern at the scale of the whole region, with a longitudinal fault family (trend N150°–N170°) and a transverse one (trend N50°–N80°). The strap-like structure linked to the longitudinal faults is particularly well visible on the DEM and the image along the Briançonnais zone. Individual faults recognized on the field are indicated on the SPOT view (white symbols). Local names of majors faults are ChS, South Chenailliet fault; CVx, Col Vieux fault; Dur, High Durance fault; Ebr, East Briançonnais fault; Emb, Embrunais fault; Esc, Escrains fault; FSA, Font Sancte Fault; Gui, Guil fault; Hub, High Ubaye fault; Par, Parpaillon fault; Pou, Pousterle fault; Ser, Serenne fault.



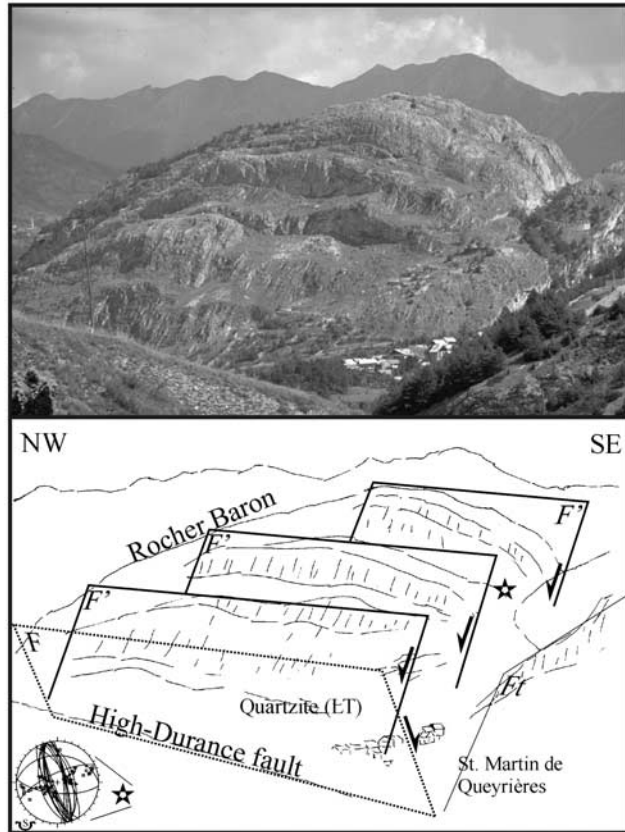


Figure 5. “Rocher Baron” site exhibiting longitudinal west dipping second-order normal faults (some hundreds of meters) conjugated with the major east dipping High Durance normal fault. The normal faults in the Rocher Baron site are well visible, being developed in Triassic quartzites (strong lithology, basal Briançonnais nappe). Moreover, microtectonic measurements (slickensides) agree with the large-scale qualitative observations of longitudinal faults (trending NNW-SSE). The data presented in the stereonet (see also the section 3.3) exhibit mainly NNW-SSE normal faults, with more or less the same number of east and west dipping faults, and some transverse normal faults oriented ENE-WSW. Note the transverse fault (Ft) to the SE of the Rocher Baron site.

corresponding paleostress inversion). Strike-slip reactivation is particularly important along the High Durance fault (Figure 9) and can be followed to the south along the Escreins fault and the Serenne fault. Typically, such reactivation has led to right-lateral motions along

longitudinal faults and left-lateral motions along transverse faults.

[13] To sum up, the qualitative kinematic analysis of the fault network has shown that it formed the last alpine tectonic phase. The fault network is made of two faults families, one longitudinal and another transverse to the belt. The two fault families are coeval. The fault network developed under brittle conditions in response to an extensional tectonic regime affecting the internal zones of the western alpine arc. It is followed by transcurrent motions, which are locally important. Thus, for the late alpine period, after the last compressive alpine tectonic phase, the Briançonnais zone overall underwent extensional tectonics associated with transcurrent movements.

3.3. Paleostress Computation

[14] In this section, we address the problem of late alpine tectonics in terms of paleostress analysis. This quantitative approach is based on the measurements of faults planes and associated slip directions. The direction of movement is given by slickensides, striae, and grooves on the fault plane. The sense of movement is generally given by calcareous fibers (calcareous lithology), drag-folds, steps impressed in the plane by striator objects, riedel criteria, etc.

3.3.1. Method

[15] We use the conventional notations σ_1 , σ_2 , and σ_3 for the main stresses axes (maximal, intermediate, and minimal, respectively) and $\Phi = (\sigma_2 - \sigma_3)/(\sigma_1 - \sigma_3)$ the shape ratio of the stress ellipsoid [e.g., *Angelier, 1975; Angelier and Mechler, 1977; Ritz, 1991; Ritz and Taboada, 1993*]. The inversion of microtectonic data provides the reduced stress tensor, as the magnitudes of the stresses and the isotropic part of the stress tensor cannot be reached using this kind of inversion [*Sassi and Carey-Gailhardis, 1987; Angelier, 1989*]. The numerical methods for the paleostress tensor inversion [e.g., *Carey and Brunier, 1974; Angelier and Goguel, 1979; Etchecopar et al., 1981; Angelier, 1984; Pfiffner and Burkhard, 1987; Angelier, 1990*] are based on the *Wallace* [1951] and *Bott* [1959] principle, after which the striae direction and the direction of the tangential stress on the fault plane are parallel. It is necessary to make some basic assumptions: the rock volume should be homogeneous and isotropic, the stress field should be uniform (notion of “mean state of stress”) and steady during a given tectonic phase, slip along fault planes should be free, deformations should be incremental, and rotation should be negligible. These assumptions are not all verified in real cases, particularly the state of stress varying with the heterogeneity of the rocks. Nevertheless, the mean state of stress is justified a posteriori by the coherency of the results

Figure 4. (opposite) (a) Fault network (not interpolated) surveyed in the Briançonnais-Ubaye-Queras area using field work and remote sensing documents (aerial photography, DEM, SPOT view, see section 3.1 for the geometric description). The sites surveyed in term of paleostress (see section 3.3) are plotted with their five-letter code (Table 1). (b) Interpolation of the fault network mapped in Figure 4a in the southwestern alpine tectonic framework. The names of the main late alpine faults are Arg, Argentera fault; Ber, Bersezio fault; Cer, Cervières fault; Cha, Chaberton fault; ChN, north Chenaillet fault; ChS, south Chenaillet fault; Cla, Clarée fault; CVx, Col Vieux fault; Dur, Durance fault; Ebr, East Briançonnais fault; Emb, Embrunais fault; Esc, Escreins fault; Fsa, Font Sancte fault; Gui, Guil fault; GRc, Gran Roc fault; Hub, High Ubaye fault; Jan, Janus fault; Mal, Malrif fault; Par, Parpaillon fault, Pou, Pouterle fault; Rbr, Roche Brune fault; Ser, Serenne fault; Val, Valloire fault.

[Angelier and Mechler, 1977]. These methods are thus applicable in a relatively small rock volume, homogeneous enough to come close to the basic hypotheses. Here, we applied the direct inversion method (INVD) developed by Angelier [1990], which analytically solves the inverse problem of the paleostress tensor. It is based on the minimization of a function of the angle between the measured striae and the computed one. The accurate analysis of each polyphased site (normal and strike-slip motions) allowed the recognition in the field of the local relative timing of the different sets of slickensides. Thus we did not proceed to automatic classification of the data to extract different tensor at a given site. From a numerical point of view, each paleostress tensor inversion using the

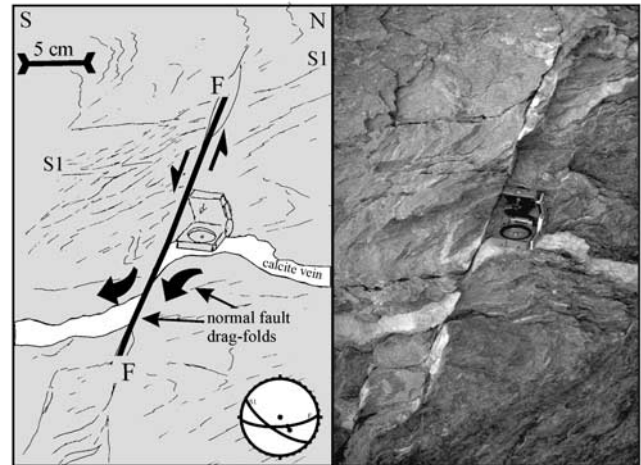
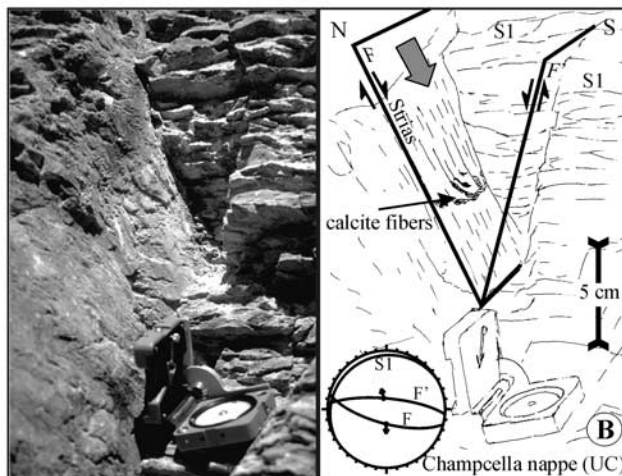
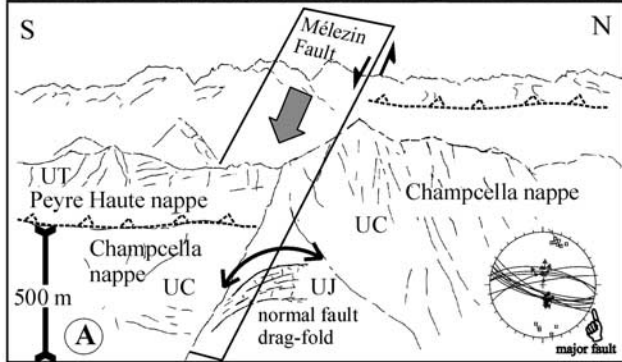


Figure 7. Example of small-scale extensional structure in the High Ubaye area. The calcite vein gives the sense of motion.



INVD method has been associated to a research of the domains for σ_1 and σ_3 using the right diehda method. The quality of each inversion is estimated by the statistical parameters of the distribution of the angles between the real striae (measured) and the computed one.

3.3.2. Data Analysis

[16] Typical paleostress tensors computed in the studied area are plotted on Figure 10. Note that the histograms

Figure 6. (opposite) Melezin site, SE of Briançon providing a typical example of transverse normal fault and associated structural objects. (a) Main structure of a major normal fault showing a throw of several hundreds of meters, which clearly postdates the nappe tectonics of the Briançonnais zone as it affects the nappe contact between the lower and the middle Briançonnais nappe, so-called Champcella and Peyre Haute nappes, respectively. The lower Triassic dolomite of the base of the Peyre Haute nappe (to the south) is thus at the same level as the upper Cretaceous calcites of the Champcella nappe (to the north). Another large-scale structural object showing the importance of the normal displacement along this fault is a large anticline drag-fold developed in upper Jurassic limestones of the Champcella nappe, immediately to the north, below the fault. Data collected in this area are shown on the stereonet. They exhibit E-W trending normal microfaults (slickenside measurements) and south dipping (as the major one) as well as north dipping (conjugated planes). (b) These kinds of mesofaults to microfaults (some centimeters to some meters) also well developed in the calcschistes, where one can observe conjugated E-W trending microfaults (western side of the Melezin pike). The planes bear witness of normal motion (striae, calcareous fibers). Small drag-folds are also developed in the almost horizontal schistosity planes. These small structures clearly establish the relative chronology between the schistosity development associated to compressional alpine phases (first) and the brittle extension (second).

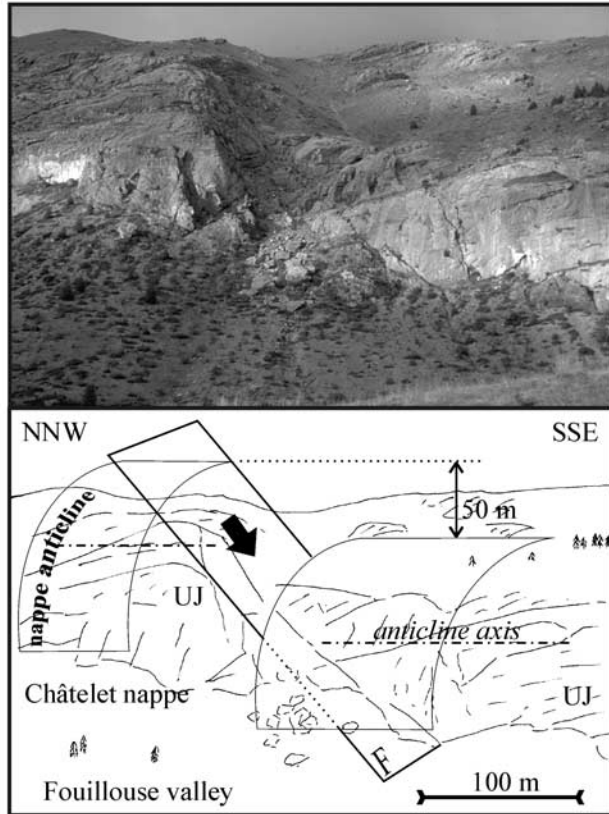


Figure 8. Example of large-scale normal fault in the High Ubaye area. The nappe-scale anticline is crosscut by the normal fault, which shifts the fold axis.

(statistical distribution of the differential angle between the measured striae and the computed ones) are important quality estimators for each paleostress inversion. A good inversion is characterized by angles lower than 20° . The average angle and the standard deviation given on the top of the histogram also allow judgment of the quality of the inversion. The whole database of paleostress tensors used in this study is shown in Figure 11. The corresponding parameters are given in Table 1, including the quality estimators: average angle and standard deviation. The striated fault planes we studied on the field mainly exhibit extensional and strike-slip movements. Thus our large-scale qualitative observations are coherent with these microtectonic quantitative results. Two main sorts of paleostress tensors have been computed: extensive, respectively transcurrent, with σ_1 , respectively σ_2 , close to the vertical axis. The tensors presented in Figure 10 illustrate typical paleostress tensors for the studied area along the Briançonnais zone. The two first ones (codes NEUFC and TURGE) belong to the extensive type of tensors, whereas the last one (code PCHAT) belongs to the transcurrent type of tensor. The NEUFC tensor, in the High Ubaye region, exhibits a NW-SE σ_3 axis, which corresponds to normal movement along longitudinal faults. The distribution of the

strikes is pretty large, showing a well constrained tensor. The quality of the inversion is good, with only two angles higher than 20° . The TURGE site, located to the SE of Briançon, shows a smaller distribution of fault directions, around an E-W mean strike. Nevertheless, there is a good agreement between the INVD inversion and the right diebra method. Moreover, the histogram is very good, as are the average value (8.8°) and standard deviation (6.3°). This paleostress tensor is mainly controlled by transverse faulting, which explains the N-S σ_3 orientation. The third tensor in the PCHAT site (High Ubaye region) shows a bimodal distribution of the fault directions, corresponding to the longitudinal and transverse fault families. This transcurrent tensor provides an E-W extension associated to a N-S compression, which is characteristic of right-lateral motions along the longitudinal faults conjugated with left-lateral motions along the transverse ones. Here also, the quality of the inversion is very good (average angle of 7.5° with a

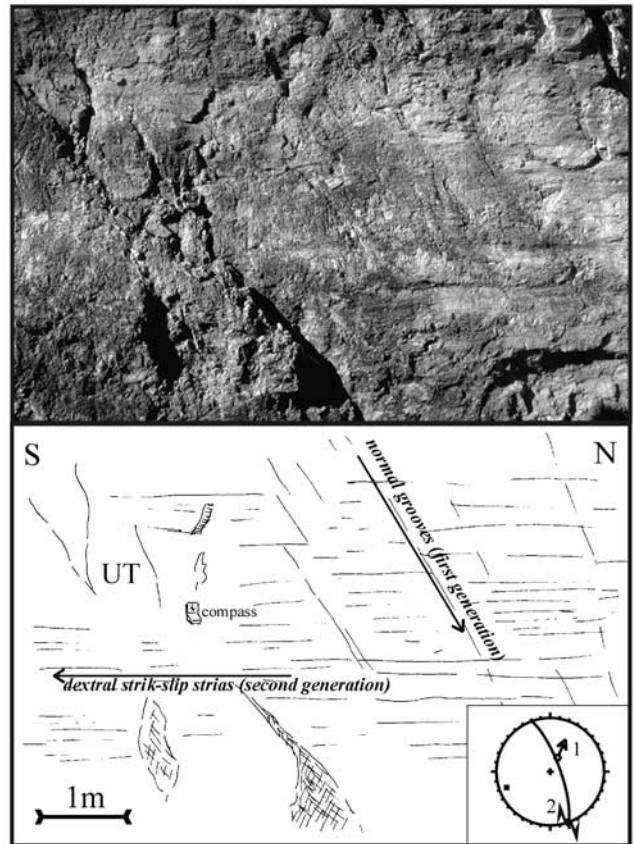


Figure 9. Large fault plane in the Durance valley, belonging to the High Durance fault zone. The fault plane exhibits both quite large grooves, associated with the first mainly normal displacements on the fault, and thinner almost horizontal striates, posterior to the grooves, associated to strike-slip reactivations. The sense of the strike-slip movement is dextral. The stereonet gives the measurements corresponding to the oblique normal grooves (1) and to the horizontal dextral striates (2).

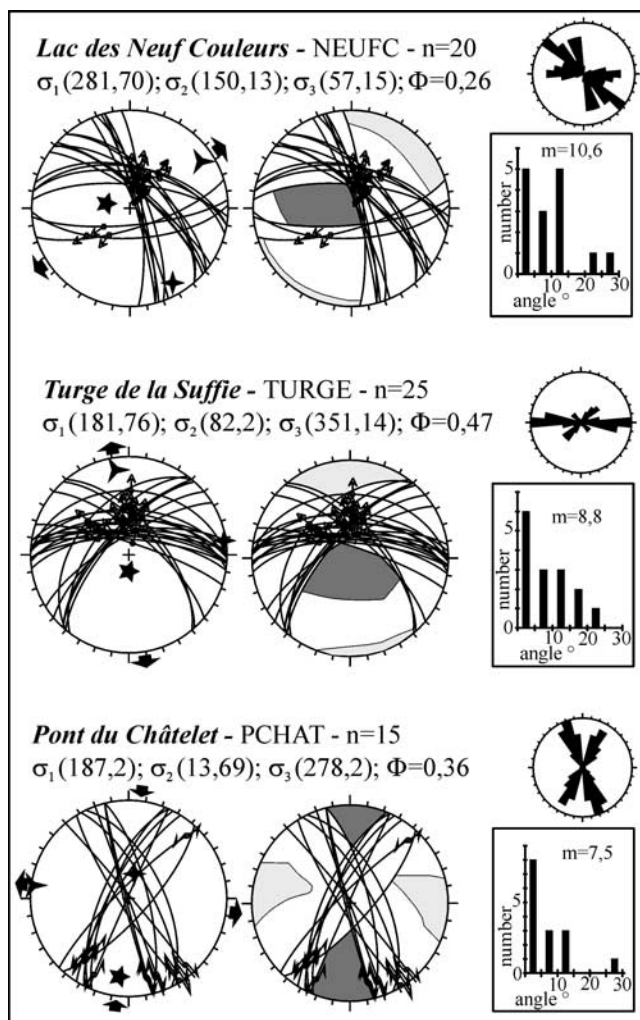


Figure 10. Typical paleostress tensors computed in the studied area (Schmidt stereonets, lower hemisphere). The left stereonet represents the paleostress tensor computed using the INVD method [Angelier, 1990], with the faults great circle projection and slip projection (arrows), and the three main stress axes σ_1 , σ_2 , σ_3 , symbolized by the five-branch, four-branch, three-branch stars, respectively. The middle stereonet gives the right diedra result, with the same fault and slip projection and the potential area for σ_1 and σ_3 (dark gray and light gray respectively). The small stereonet on the right gives the statistical distribution of the faults' strikes, allowing estimation of the spatial repartition of the database. The histogram gives the statistical distribution of the angle between the measured striae and the computed ones. This histogram is an important quality estimator for each paleostress inversion.

standard deviation of 7.9°). In term of relative chronology, the careful analysis of the 12 polyphased sites that we studied on the field, has shown that the transcurrent motions were younger than the normal ones. Nevertheless, this relative chronology remains local, because the great majority of the sites were not polyphased; that is, they exhibited

only normal or transcurrent motions. The relationships between the microtectonic measurements (paleostress inversion) and the large-scale faults have been locally illustrated by Sue and Tricart [1999, 2002]. A good example of close relationships between large-scale structures and measurements are the normal faults of the Rocher Baron (code ROBAR) and Melezin (code MLZSU) sites presented above (Figures 5 and 6). The corresponding faults/striae data are inverted and reported in Figure 11 (tensors 52 and 45, respectively). They exhibit good agreements with the large-scale structures (see section 3.2). Thus regionally there is a good coherency between the structures observed in the field and the microtectonic measurements.

[17] Sixty-six paleostress tensors have been computed over the whole studied area. They represent around 1300 data (fault/striae couple measurements). Each tensor can be localized using the general map of the area Figure 4a. The corresponding 66 stereonets, with the faults and slip projections and the paleostress axes representations (stars) are plotted on Figure 11. We obtained classically a subvertical stress axis and two subhorizontal ones. On the maps, we only projected the subhorizontal ones, i.e., σ_3 and σ_2 (σ_3 and σ_1 , respectively) for the extensional (respectively transcurrent) regimes. The paleostress maps shown in Figure 12 give an overview of the regional paleostresses fields associated to the normal (Figure 12a) and transcurrent (Figure 12b) regimes, respectively. For clarity of the maps, we separated the two subsets of tensors according to the local relative chronology found in the 12 polyphased sites (strike slip after extension).

[18] The horizontal axes of the tensors associated with the extensional paleostress field (σ_1 vertical) are plotted in Figure 12a. The trend of σ_3 (extension) varies from E-W along the western edge of the Briançonnais zone close to the CPF to NW-SE in the central part of the Briançonnais zone and in the Piemont zone. The longitudinal faults, which were preponderant in the large-scale analysis, actually control the E-W extension in the western part. In the central and eastern sectors of the study area the transverses faults seem to be preponderant in terms of paleostress analysis, as they control the NW-SE trend of the extensional axes. The longitudinal faults delimit strap-like zones, into which the extension develops mainly along transverse faults. Overall, at a regional scale, we obtain a multitrend extensional regime. The quite low Φ ratios (0.35 of average value) computed for these tensors can explain the important variations found in the trend of σ_3 . Actually, low Φ ratios can be associated to close σ_2 and σ_3 magnitudes, which explains rapid spatial permutation between σ_2 and σ_3 and thus the observed regional paleostress field. Indeed, the trends of σ_3 (σ_2 , respectively) in the western part are close to the trend of σ_2 (σ_3 , respectively) in the central and eastern sectors.

[19] The horizontal axes of the tensors associated to the transcurrent paleostress field (σ_2 vertical) are plotted in Figure 12b. The trend of σ_3 appears very steadily NW-SE to WNW-ESE. The Φ ratios are higher than for the extensional paleostress field (0.56 of average value). This paleostress field is very homogeneous in the whole study area,

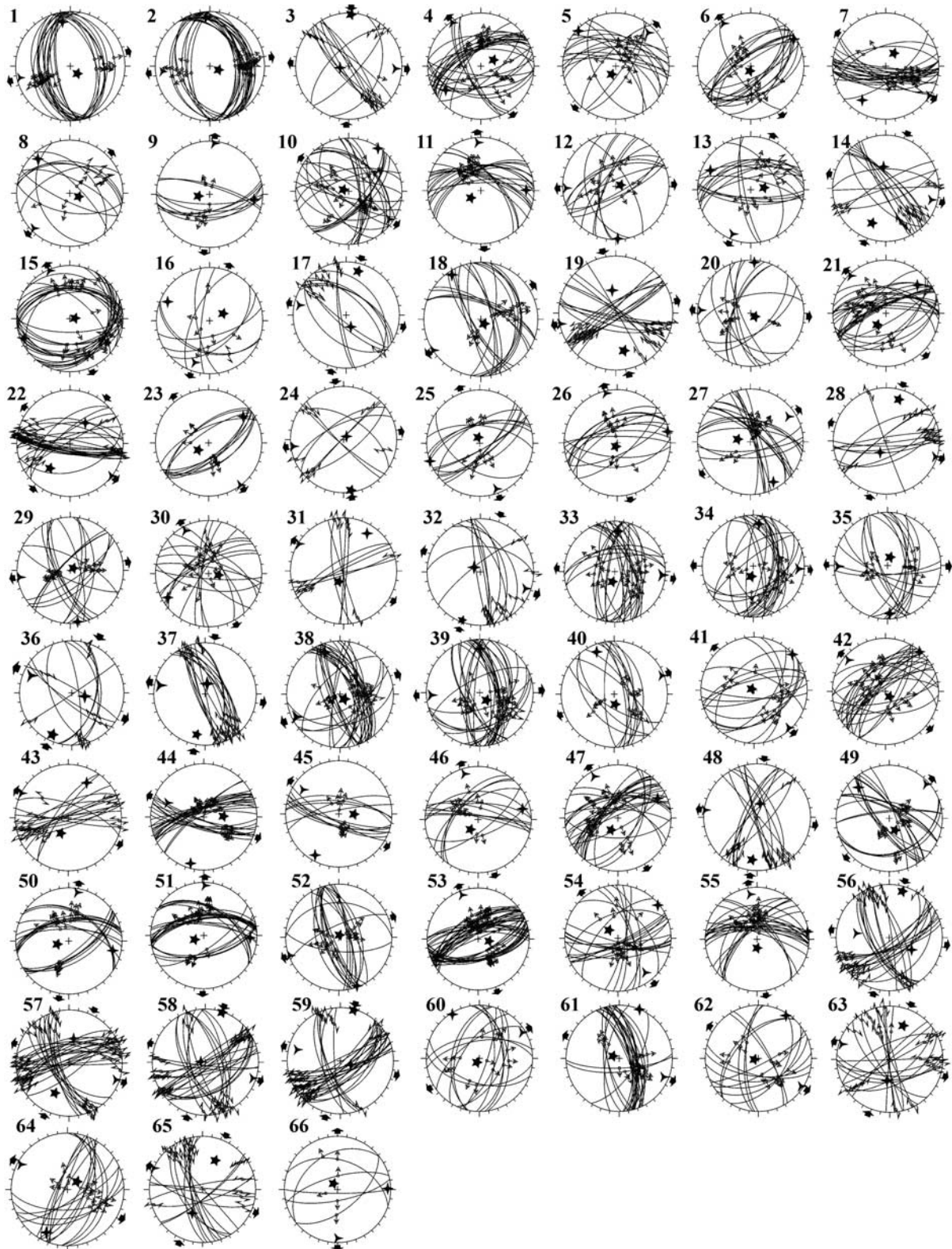


Figure 11. The complete database of 66 paleostress tensors (direct inversion method, see section 3.3.1). The stereonet numbers refer to the Table 1.

Table 1. Parameters of the 66 Paleostress Tensors^a

No.	Site	Code	Latitude	Longitude	<i>N</i>	σ_1	σ_2	σ_3	Φ	Gl	T	<i>m</i>	SD
1	Barre du Treuil nord	BDTNO	44°43.88'N	6°31.25'E	30	142.77	349.18	258.6	0.6	1	N	4.7	4.3
2	Barre du Treuil sud	BDTSU	44°42.88'N	6°31.74'E	25	108.83	356.3	265.6	0.4	1	N	4.8	3.2
3	Bersezio	RUBUR	44°23.81'N	6°58.39'E	12	2.3	260.76	93.13	0.8	1	D	17.8	8.4
4	Bouchouse	BOUCH	44°41.41'N	6°56.95'E	30	64.69	236.21	327.3	0.2	1	N	7.5	6.8
5	Cervière	CERVI	44°53.17'N	6°45.03'E	18	208.76	313.4	44.14	0.3	1	N	9.7	9.8
6	Chaberton	CHABE	44°58.38'N	6°45.54'E	21	193.83	58.5	327.5	0.4	1	N	9.5	7.1
7	Chambeyron	CHAMB	44°32.48'N	6°50.08'E	23	32.67	214.23	124.1	0.3	1	N	11.4	6.9
8	Chenaillet nord	CHENO	44°55.52'N	6°45.18'E	10	111.76	317.13	226.6	0.4	1	N	14.0	6.0
9	Chenaillet sud	CHESU	44°54.74'N	6°45.16'E	10	261.73	97.17	5.4	0.3	1	N	11.0	6.0
10	Clot de Malamort	MALAM	44°42.71'N	6°38.60'E	36	287.81	34.3	125.8	0.2	1	N	9.2	8.5
11	Col de la Ricelle	COLRI	44°56.05'N	6°32.00'E	19	234.71	89.16	356.10	0.3	1	N	7.2	5.3
12	Col des Peygus	PEYGU	44°49.51'N	6°44.42'E	13	66.78	182.5	273.11	0.2	1	N	14.6	9.2
13	Col du Longet	LONGE	44°39.00'N	6°56.92'E	16	81.70	296.17	202.11	0.2	1	N	12.9	8.0
14	Col sans Nom	COLSN	44°29.33'N	6°50.46'E	15	202.3	354.57	104.13	0.6	1	D	8.6	7.4
15	Collet du Peyron	CPEYR	44°46.58'N	6°37.47'E	30	84.82	247.7	337.3	0.2	1	N	11.7	8.9
16	Crête desCrouzas	CROUS	44°43.43'N	6°39.31'E	8	62.67	294.15	199.17	0.4	1	N	15.0	9.8
17	Crête desCrouzas	CROUS	44°43.43'N	6°39.31'E	10	15.16	157.70	282.11	0.5	2	D	16.5	9.0
18	Croix de la Salcette	CRXSA	44°50.18'N	6°33.05'E	19	143.82	327.8	237.1	0.4	1	N	10.3	9.8
19	Croix de la Salcette	CRXSA	44°50.18'N	6°33.05'E	20	169.32	353.58	260.2	0.5	2	D	7.3	7.9
20	Fouillouse	FOUIL	44°33.22'N	6°48.02'E	11	130.82	4.5	274.6	0.4	1	N	10.4	7.0
21	Gros ouest	GROOU	44°39.56'N	6°40.53'E	27	218.68	48.22	317.4	0.2	1	N	11.0	7.8
22	Gros ouest	GROOU	44°39.56'N	6°40.53'E	27	219.39	37.50	128.1	0.8	2	D	11.3	9.6
23	Janus est	JANES	44°56.03'N	6°44.31'E	11	236.70	53.19	143.1	0.5	1	N	5.0	2.8
24	Janus est	JANES	44°56.03'N	6°44.31'E	8	172.4	43.83	262.5	0.7	2	D	14.5	9.2
25	Janus ouest	JANOU	44°56.29'N	6°45.21'E	13	343.81	250.0	160.9	0.4	1	N	9.8	6.6
26	Lac des Cordes	LCORD	44°50.46'N	6°46.13'E	13	204.84	77.4	347.5	0.4	1	N	10.5	7.7
27	Lac des Neuf Couleurs	NEUFC	44°34.28'N	6°46.35'E	20	281.70	150.13	57.15	0.3	1	N	10.6	8.3
28	Lac des Neuf Couleurs	NEUFC	44°34.28'N	6°46.35'E	12	16.20	208.70	108.4	0.6	2	D	11.4	10.2
29	Lausette	LAUSE	44°51.35'N	6°39.91'E	17	55.84	172.3	262.5	0.3	1	N	8.8	5.7
30	Laval	LAVAL	44°56.10'N	6°52.64'E	22	175.75	84.0	354.15	0.4	1	N	11.7	7.5
31	Maison du Roy nord	MROYN	44°41.54'N	6°43.78'E	10	32.18	204.72	301.2	0.8	1	D	9.4	9.7
32	Oréac centre	ORECE	44°48.10'N	6°30.25'E	17	200.2	310.83	111.7	0.8	2	D	8.5	7.3
33	Oréac centre - a	ORCEA	44°48.10'N	6°30.28'E	23	195.77	3.15	93.4	0.3	1	N	12.0	9.2
34	Oréac centre - b	ORCEB	44°48.10'N	6°30.26'E	16	199.75	2.14	93.4	0.1	1	N	11.4	8.5
35	Oréac est	OREES	44°47.78'N	6°30.67'E	10	15.77	178.13	269.4	0.2	1	N	12.6	9.1
36	Oréac est	OREES	44°47.78'N	6°30.67'E	10	203.5	96.73	295.16	0.2	2	D	17.8	9.8
37	Oréac ouest	OREOU	44°47.80'N	6°30.69'E	26	192.15	18.75	283.1	0.5	2	D	13.5	8.8
38	Oréac ouest - a	OROUA	44°47.71'N	6°31.29'E	31	122.80	343.7	252.6	0.3	1	N	9.5	8.5
39	Oréac ouest - b	ORoub	44°47.71'N	6°31.28'E	32	144.75	0.12	268.8	0.2	1	N	11.2	7.9
40	Parpaillon	PARPA	44°29.81'N	6°40.65'E	13	176.74	337.15	69.5	0.2	1	N	14.0	8.5
41	Petit Puy	PTPUY	44°49.95'N	6°38.74'E	15	298.85	47.1	137.4	0.4	1	N	9.0	7.7
42	Pic de Beaudouis	BEAUD	44°49.12'N	6°41.34'E	26	142.80	41.2	310.1	0.3	2	N	15.5	8.1
43	Pic des Houerts	HOUER	44°35.26'N	6°46.95'E	16	207.29	62.56	304.18	0.7	1	D	14.8	10.4
44	Pic du Mélezin ouest	MLZOU	44°50.53'N	6°37.91'E	30	91.52	232.32	331.14	0.2	1	N	8.6	6.1
45	Pic du Mélezin sud	MLZSU	44°49.96'N	6°38.18'E	12	97.62	258.28	349.28	0.1	1	N	9.0	7.2
46	Pic du Panestrel	PSTRL	44°34.76'N	6°47.51'E	14	218.71	76.15	343.11	0.2	1	N	8.5	6.3
47	Pont du Châtelet	PCHAT	44°32.40'N	6°47.27'E	29	210.69	64.18	330.11	0.1	1	N	14.3	8.8
48	Pont du Châtelet	PCHAT	44°32.40'N	6°47.27'E	15	187.2	13.69	278.2	0.4	2	D	7.5	7.9
49	Prorel	PRORE	44°54.32'N	6°33.85'E	20	154.70	315.19	47.6	0.2	1	N	9.0	6.6
50	Roche Motte est	RMOES	44°50.08'N	6°36.73'E	19	252.72	102.16	10.8	0.2	1	N	7.7	7.4
51	Roche Motte ouest	RMOOU	44°50.40'N	6°37.05'E	26	245.75	93.14	1.6	0.3	1	N	8.7	9.9
52	Rocher Baron	ROBAR	44°48.48'N	6°34.19'E	20	15.86	159.3	249.2	0.4	1	N	10.0	8.5
53	Rocher Blanc est	RBLES	44°54.50'N	6°33.26'E	45	101.72	247.15	340.9	0.5	1	N	9.3	6.4
54	Rocher Blanc ouest	RBLou	44°54.50'N	6°32.54'E	22	312.71	50.3	141.18	0.4	1	N	9.7	6.7
55	Turge de la Suffie	TURGE	44°49.73'N	6°46.84'E	25	181.76	82.2	351.14	0.5	1	N	8.8	6.3
56	Val d'Escrains - Pégier	ESCPE	44°38.36'N	6°40.62'E	25	16.10	118.60	277.27	0.2	1	D	7.6	5.3
57	Val d'Escrains - Rima	ESCRI	44°38.57'N	6°41.39'E	34	205.38	10.52	110.7	0.9	1	D	6.0	6.5
58	Val d'Escrains nord	ESCNO	44°38.10'N	6°42.02'E	30	19.1	276.83	108.7	0.4	1	D	9.0	7.9
59	Val d'Escrains sud	ESCSU	44°37.77'N	6°42.98'E	29	15.2	111.73	284.17	0.4	1	D	7.3	5.5
60	Vallée de Freissinières	FREIS	44°45.65'N	6°32.14'E	15	213.83	329.3	59.7	0.3	1	N	15.8	9.4
61	Vallée du Fournel	FOURN	44°47.77'N	6°32.66'E	25	290.80	33.0	113.10	0.4	1	N	11.7	7.8
62	Vallon de Baraigne	BARAI	44°33.31'N	6°49.58'E	15	256.83	33.5	123.5	0.4	1	N	14.4	7.8
63	Vallon de Baraigne	BARAI	44°33.31'N	6°49.58'E	21	21.33	188.57	287.6	0.7	2	D	15.7	9.1
64	Vallon de Mary	VMARY	44°34.21'N	6°51.75'E	17	50.73	206.16	298.7	0.4	1	N	10.5	7.7
65	Vallon des Houerts	VHOUE	44°34.73'N	6°49.45'E	17	24.40	203.50	293.1	0.8	1	D	9.8	5.6
66	Vallon Laugier	VLAUG	44°35.67'N	6°45.05'E	6	325.79	89.6	180.9	0.4	1	N	10.3	6.2

^aSee Figure 11 for the corresponding stereonet: No., number of the tensor; site, name of the measurement site; code, five-letter code (see Figure 4 for the location); latitude and longitude of the site; *N*, number of fault/striae measurements; σ_1 , σ_2 , σ_3 , principal stress axes (azimuth, dip); Φ , shape ratio of the stress ellipsoid; Gl, local generation of the tensor; T, type of tensor (N, normal; D, strike slip); *m*, average value of the differential angles between measured and computed striae; SD, standard deviation of the differential angles.

from the Ruburent site to the south up to the Oreac area to the north, although the two northernmost tensors (Croix de la Salcette and Janus sites) have E-W trending σ_3 . This paleostress field is globally linked to the right-lateral transcurrent movements along the longitudinal faults conjugated to the left-lateral transcurrent movements along the transverse ones. They appear to be very important along the Durance, Escrein, and Bresezio faults, which worked as a major strike-slip fault zone in the western Alps, immediately east of the CPF, in response to a remarkably homogeneous paleostress field.

[20] Statistical analysis of the whole paleostress tensors database allows precise comparison of the normal and transcurrent regimes. The main stress axes of the tensors are plotted on the stereonet in Figure 13. There is one stereonet for each axis (σ_1 , σ_2 , and σ_3) and for each kind of tensor (normal and transcurrent). This statistical analysis has been made using the STEM software, an improved version of the Maccschmidt software [Pécher, 1989]. Distribution of the normal tensors (σ_1 vertical, stereonets A, B, C) is bimodal considering the σ_2 and σ_3 axes (stereonets B and C, respectively). The axes are grouped in two clusters drawn in gray and black, respectively. This corresponds to the regional distribution observed in map (see above). The B and C stereonets and the computed best axes for the two σ_2 and the two σ_3 clusters point out a clear permutation between the σ_2 and σ_3 axes of each cluster. The best axes are (63, 1) and (340, 7) for σ_2 and (335, 3) and (254, 1) for σ_3 . This permutation is probably associated to the low values of the Φ ratio concerning the normal tensor (left histogram, Figure 13). It appears that a multitrend extension controlled the tectonic extensional regime, leading rapid spatial permutation between σ_2 and σ_3 . The transcurrent tensors (σ_2 vertical, stereonets D, E, F) exhibit a very steady distribution, linked to the higher Φ ratio values (right histogram, Figure 13). The associated σ_3 best axis is (286, 3). It is 30° far from the σ_3 distribution of the normal tensors, although the corresponding maps showed qualitatively a quite good correspondence between them. The difference between the σ_3 best axes may come from the regional statistics, which integrate the distribution of σ_3 for the normal and transcurrent tensors over the whole studied area. Actually, the σ_3 directions associated with the normal and transcurrent tensors remain very steady in given local areas where several polyphased sites have been investigated, such as in the southern Ubaye area. This suggests a strong tectonic relationship between extensional and transcurrent regimes.

3.4. Extensional Versus Transcurrent Tectonics in the Southwestern Internal Alps

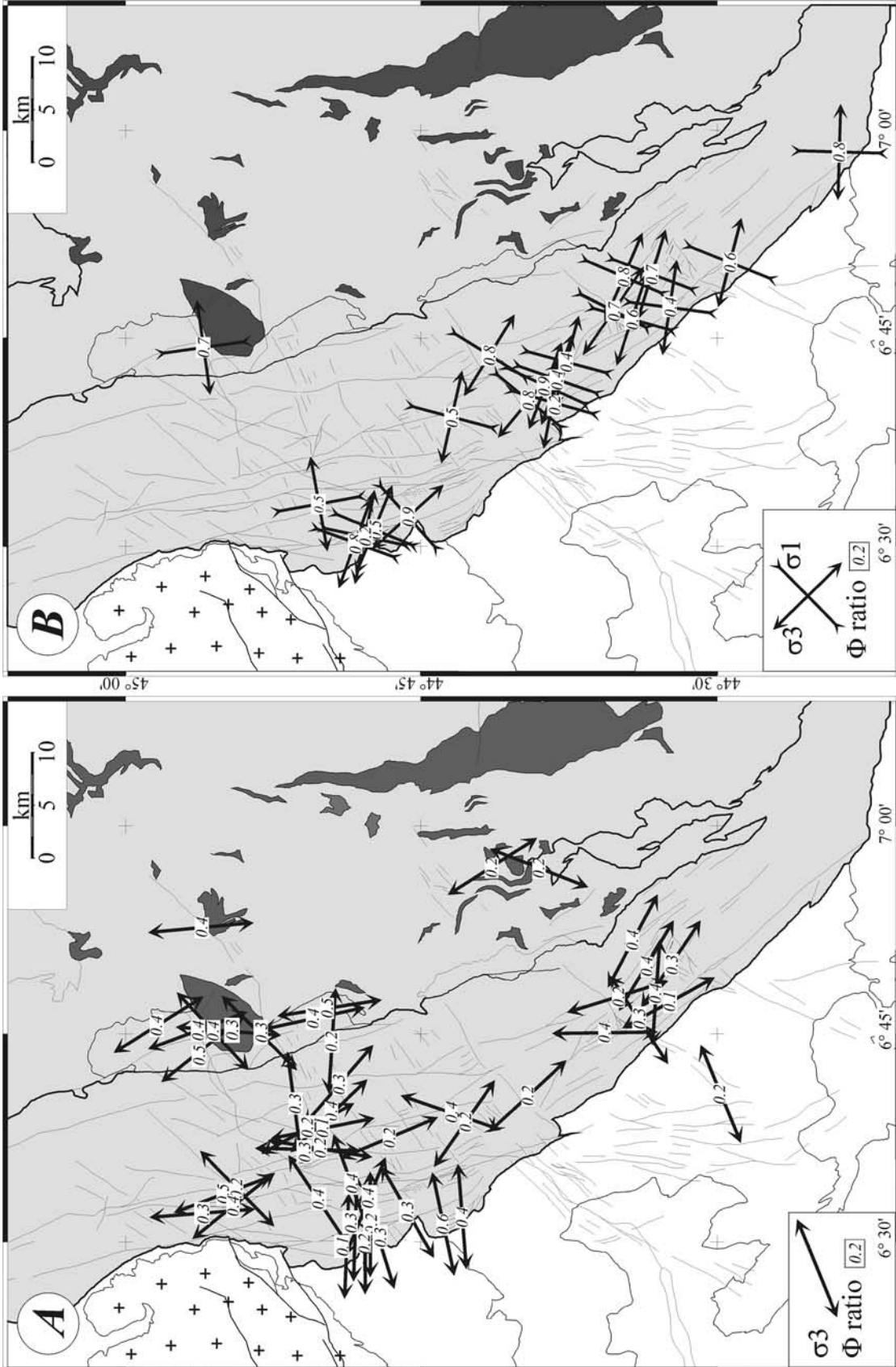
[21] The combination of different scale analyses allowed us to precisely characterize the late alpine brittle deformation. Note that the mapping of the fault network is consistent with the outcrop analyses and with the paleostress inversion. The direct inversion of microtectonic data allowed us to constrain the paleostress fields over a wide area of the southwestern Alps. We described a multitrend extensive paleostress field, dominated by E-W and NNW-SSE exten-

sion. The local transcurrent movements, corresponding to reactivation of normal faults, bear witness to the WNW-ESE σ_1 direction. Actually, the transcurrent paleostress field is closely linked to the normal paleostress field, considering the geometry of the faults implied as well as the paleostress field. A permutation between σ_1 and σ_2 axes roughly allows shifting from the extensional paleostress field to the transcurrent one. We propose that the extensive and transcurrent paleostress fields resulted from the same single tectonic regime, which is overall transtensive. Oscillations and/or instabilities in space and time into this single global transtensional tectonic regime may have led to such permutation in the type of resulting deformation, from extension to transtension and then strike-slip motions. To strengthen this interpretation, the analysis of the present-day tectonics of this area points out mainly extensive tectonics, with a small transcurrent component (see below). The late alpine tectonic regime, resulting in the fault network studied here, has probably been globally transtensive, with oscillations between a more extensive and a more transcurrent strain-stress state.

4. Seismicity Versus Late Alpine Faulting

[22] A seismotectonic analysis of the western alpine arc, based on the data of the alpine seismics networks (Sismalp, Grenoble Observatory, France, and IGG, Genova, Italy), recently showed a large-scale active extension in the whole internal zones of the belt [Sue *et al.*, 1999]. Our purpose is here to investigate the relationship between this present-day active extension and the fault network recognized on the field and to better characterize potential active fault zones using these published data. The earthquakes map (Figure 14a) displays the seismicity of the studied area during the 1989–1997 period. This zone belongs to the Briançonnais seismic arc [Rothé, 1941], which is relatively active in the alpine tectonic context, even if the magnitude of earthquakes remains quite low (magnitudes M_L typically range from 1 to 4; see Sue *et al.* [2002] for a statistical analysis of this seismicity). Epicenters were computed using a modified version of the HYPO71 software [Lee and Lahr, 1975] to take into account secondary arrivals and station altitudes. S wave readings were included when available. Only events with root-mean-square (RMS) residual smaller than 1 s and azimuthal gap smaller than 180° are plotted. The location accuracies are around 1 km for the epicenters and 2 km for the depth [Sue, 1998]. Given the great homogeneity of the database in terms of stress analysis and following Amelung and King [1997], we can address the problem of present-day alpine tectonics using this database, although the associated deformation remains low.

[23] Earthquakes affect the upper crust in its first 15 km (brittle layer) and are concentrated in the 0–10 km depth zone. To test the relationship between this upper crust seismicity and the faults observed in the field, we superimposed the fault network on the earthquake map. It appears that earthquakes cluster mainly along the longitudinal direction, which strongly suggests the current activity of this fault family. The map presents several elongated clus-



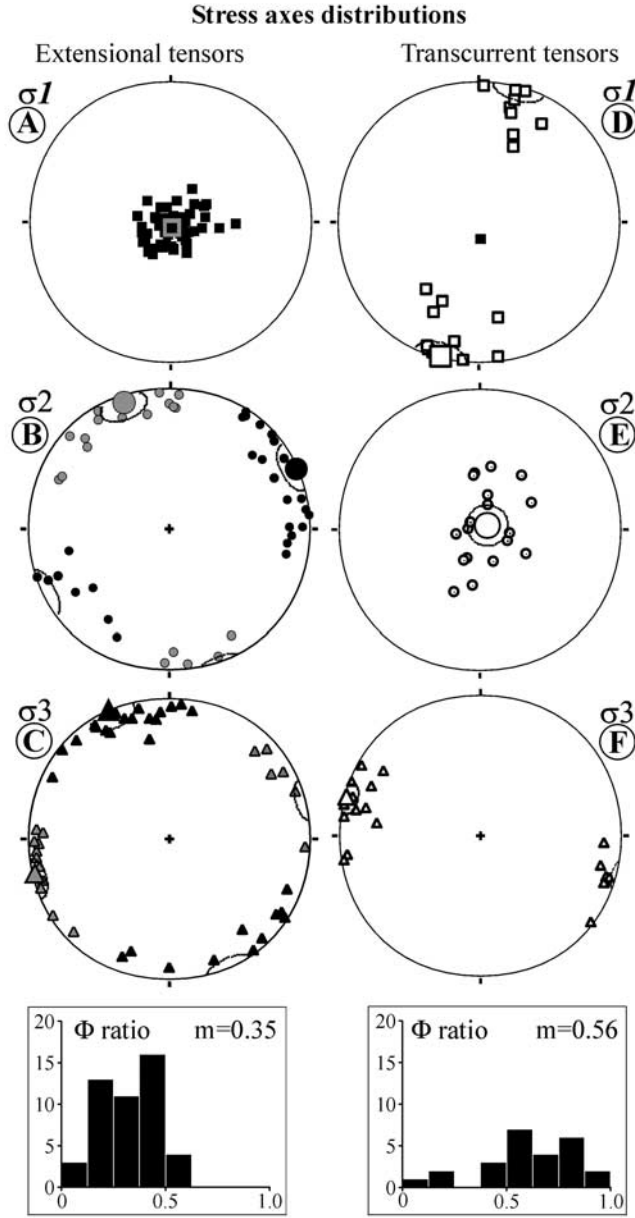


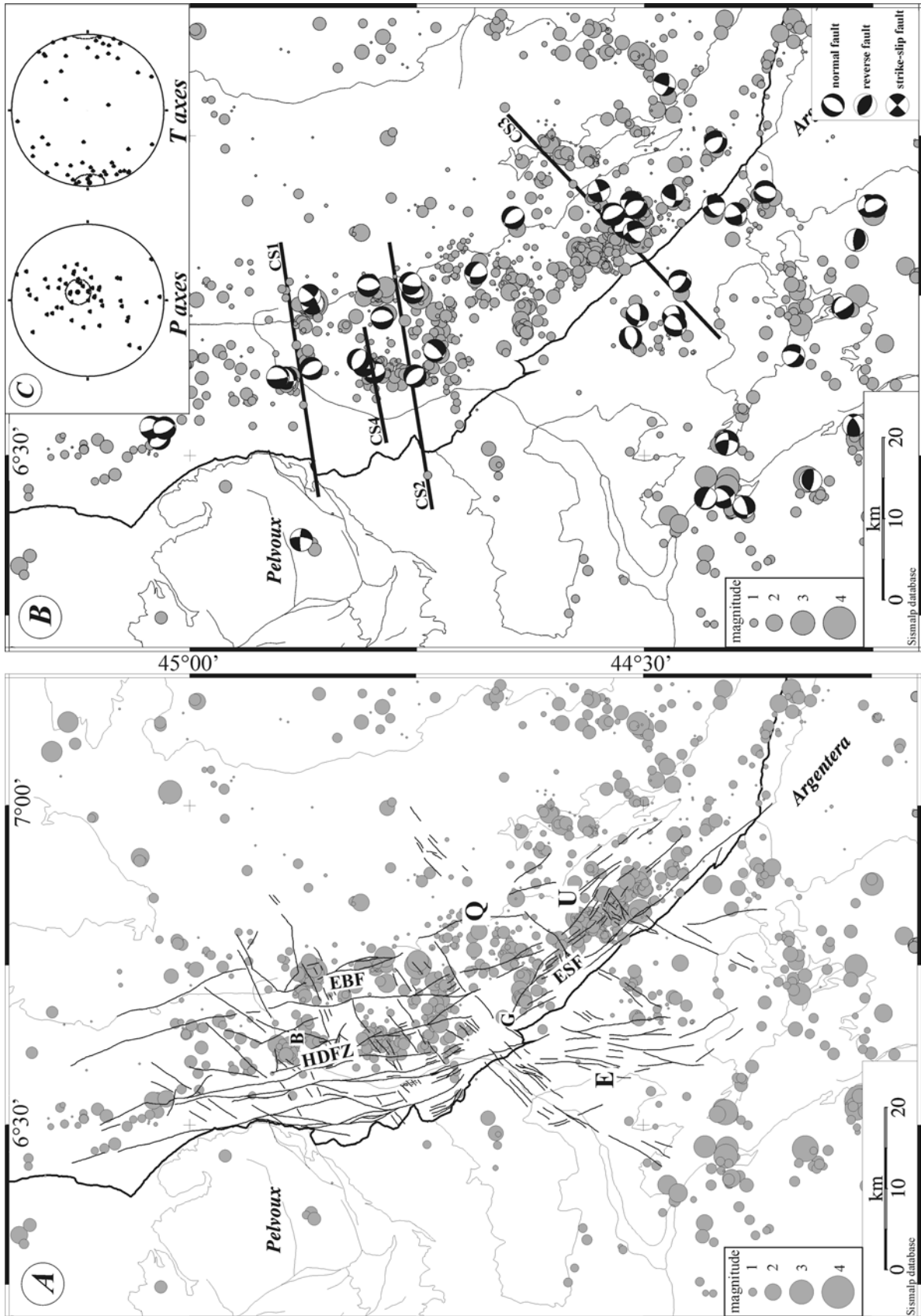
Figure 13. Statistical distributions of the principal stress axes for the (left) extensional tensors and (right) transcurrent tensors.

ters that can be related to surface-recognized faults: Between Briançon and Guillestre, the Durance fault zone appears to be quite active along a 20 km long segment; to the east, the so-called east Briançonnais fault presents the

same pattern of activity. South of Guillestre, an important cluster develops along the Escreins fault and runs through the Ubaye region, along the so-called Serenne fault. Notes that clusters elongated along the longitudinal direction are cut by some transverse alignments. This could signify that both fault families are still active: They are seismic gaps along the longitudinal faults (e.g., lack of earthquakes south of Briançon and north of Guillestre), potentially favored by transverse active faults (e.g., south and north of Guillestre). From a seismotectonic point of view the precise location of the local seismicity allowed recognition of three main longitudinal active fault zones: the Durance fault zone, which runs between the north of Briançon and the north of Guillestre (N-S); the East Briançonnais fault zone, close to the eastern limit of the Briançonnais zone, south of the Chenaillet massif (N-S); and the Escreins-Serenne fault zone, along more than 30 km southeast of Guillestre (NW-SE).

[24] The present-day tectonic regime inferred from the 50 focal solutions computed by *Sue et al.* [1999] in the study area (Figure 14b) is qualitatively very close to the late alpine tectonics deduced from the fault network and paleo-stress analysis presented above. The focal solutions are mainly extensional in the whole study area, especially along the Briançonnais zone (Briançonnais seismic arc). Only seven transcurrent solutions have been computed, and three reverse focal solutions have been computed in the southwesternmost part of the map, at the external border of the flysch nappe, in a zone probably under the tectonic influence of the external compressive and radial stress field [e.g., *Pavoni*, 1986]. In the studied area we establish a very good agreement between the late alpine faulting (mainly extensional, with some strike-slip reactivations) and the current seismic activity (around 85% normal fault and 15% transcurrent focal solutions). Figure 14c presents the spatial distribution of the whole P and T axes corresponding to the focal solutions drawn on the map Figure 14b. The global extensional regime is well illustrated by the distribution of the T axes, lying exclusively close to horizontal position. The best T axis is oriented (269, 5), showing a nearly perfect E-W extensional direction. The P axes distribution also exhibits the extensional feature of the data set, with a great concentration of P axes around the vertical axis, the corresponding best P axis being (40, 76). Only some P axes are lying in a N-S almost horizontal direction. They correspond to the few focal solutions associated to strike-slip motions: in this case, both P and T axes are horizontal. On the cross sections drawn through the Briançonnais seismic arc (Figure 15), one can recognize the active Durance fault (sections 1 and 2, see the location of the sections CS1, CS2, CS3, CS4 on Figure 14b), East Briançonnais fault (sections 1 and 2), and Escreins-Serenne fault

Figure 12. (opposite) Paleostress maps for the (a) extensional tensors (σ_1 vertical) and (b) transcurrent tensors (σ_2 vertical). In Figure 12a the extension appears regionally multidirectional, although close to the CPF it remains perpendicular to this Oligocene thrust. In Figure 12b the paleostress pattern is highly consistent with transcurrent dextral motions along the longitudinal fault system “Durance-Serenne-Bersézie”. In Figure 12a the low Φ ratios (plotted for each tensor) corroborate the multitrend characteristic of the extension, whereas in Figure 12b, the Φ ratios (above 0, 5) indicate steady principal stress directions, consistent with the regular orientations of the tensors.



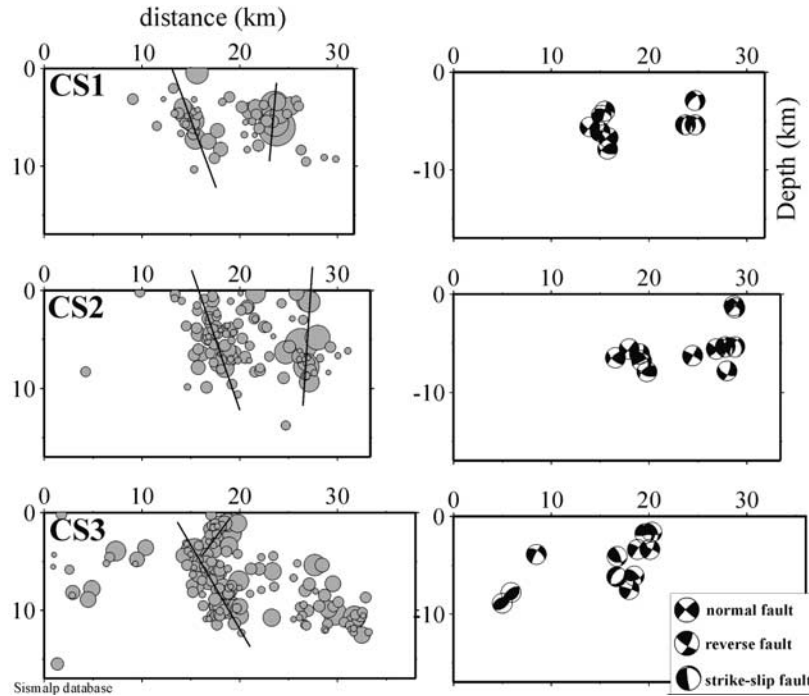


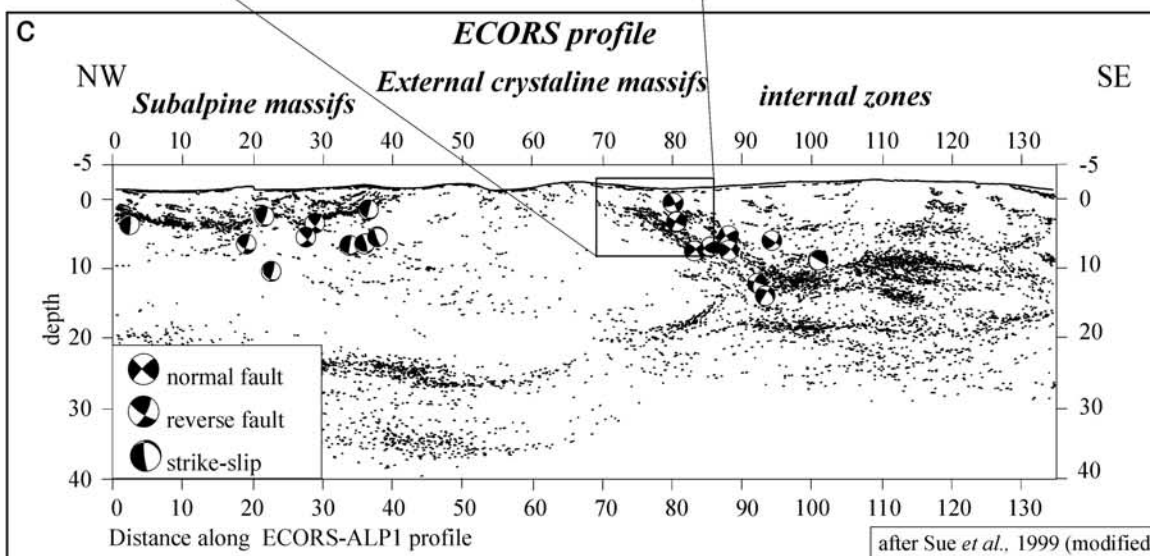
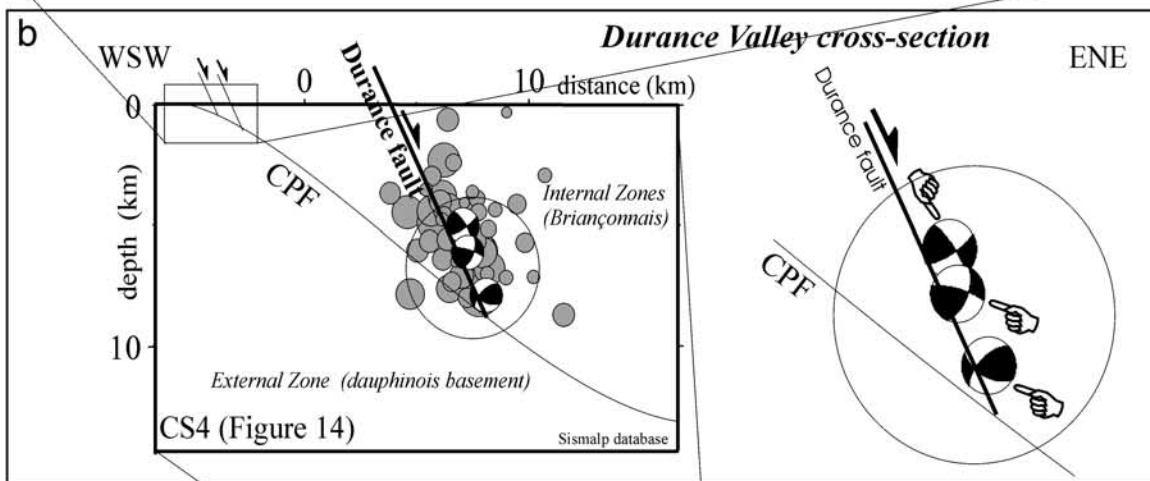
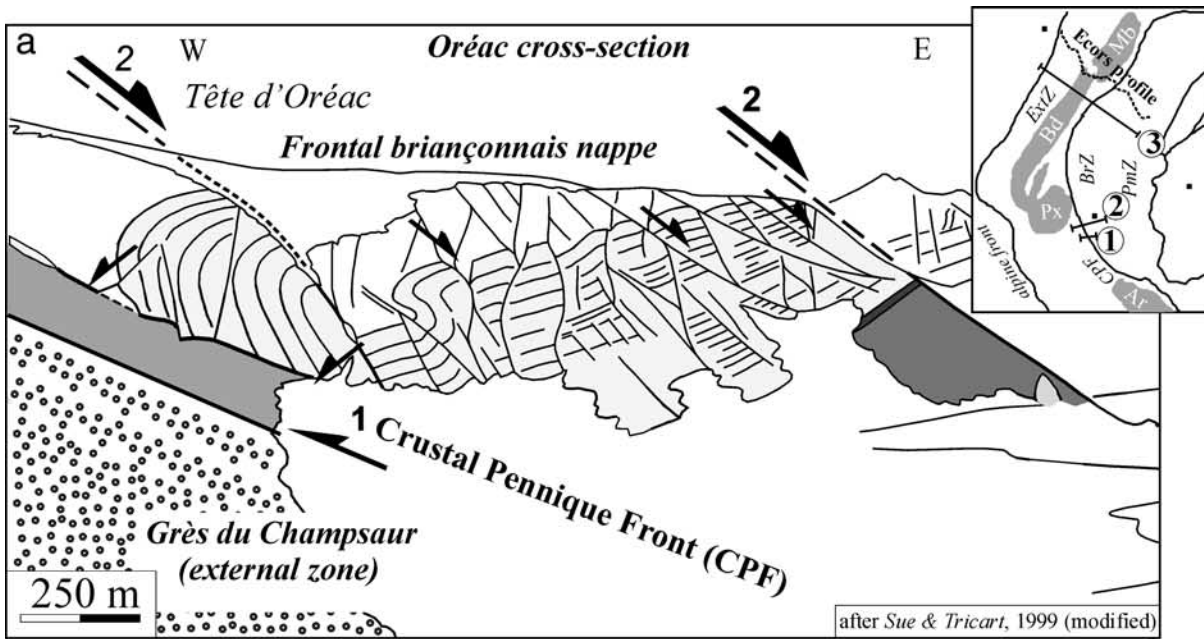
Figure 15. Seismotectonic cross sections CS1, CS2, CS3 (see Figure 14 for location). The cross sections illustrate the active faulting along the Durance (CS1 and CS2), East Briançonnais (CS1 and CS2), and Escreins-Serenne (CS3) faults recognized in surface. These faults are mapped thanks to elongated seismic clusters. On the right, the corresponding focal solutions (also view in cross section) exhibit mainly normal faulting.

(section 3). The extensional focal solutions present often focal planes compatible with the geometry of the faults mapped at the surface, as they show numerous focal plane trending N-S or NW-SE (longitudinal faults). Moreover, the strike-slip focal solutions are well compatible with the regional transcurrent tectonics inferred from the fault analysis presented above, as they show longitudinal N-S to NW-SE dextral motions conjugated with transverse E-W to NE-SW sinistral motions.

[25] The study area allows comparison of active and late alpine tectonics. We established an extensional tectonic regime, lasting during the Neogene, and still active. Both methods (structural geology and seismology) show mainly extensional tectonics, with a few strike-slip components at the regional scale, and no thrust or shortening tectonics. There is a good coherency between these two complementary approaches, allowing us to propose a continuity

through time between the late alpine faulting and the seismic activity. On cross sections the close relationship between the structural and seismotectonic approaches is underlined. Figure 16 presents thus three zoomed sections perpendicularly to the belt's trend, at three different scales: the outcrop scale (field work, Figure 16a), the upper crust scale (shallow seismotectonic cross section, Figure 16b), and the crustal scale (40 km deep, along the ECORS-CROP profile, Figure 16c). The first section (Figure 16a) in the Oreac area [Sue and Tricart, 1999] shows the branching off of the normal faults on the CPF. The second section (Figure 16b) corresponds to the section CS4 of the Figure 14b through the Durance fault. Earthquakes cluster pretty well along the track of the Durance fault, and the three focal solutions present a focal plane that may fit the dip of the Durance fault. Moreover, the seismic activity seems to stop at the depth level of the CPF, suggesting

Figure 14. (opposite) Seismotectonic maps of the studied area. (a) Relationship between the late alpine fault network (see Figure 4) and the moderate seismicity of the Briançonnais seismic arc [Sue et al., 1999, 2002]. The High Durance Fault Zone (HDFZ) along the Durance fault recognized in surface, East Briançonnais fault (EBF), and Escreins-Serenne fault system (ESF) are active and in close relationship with the mapped structures. (b) Focal solutions after Sue et al. [1999] showing mainly extensional focal mechanisms along the whole area, with some scarce strike-slip focal mechanisms. A good agreement appears between the seismotectonic analysis and the structural analysis. (c) Statistical distributions of the P and T axes of the plotted focal solutions. Best P axis (azimuth, dip), (40, 76); best T axis, (269, 5). The 95% confidence cones are symbolized by the small circles. B, Briançon; G, Guillestre; E, Embrunais; Q, Queyras; U, Ubaye; CS1-4, cross sections 1 to 4 (see Figures 15 and 16).



control of the extensional faulting by this former thrust, as in the case of the faults described in the Oreac area. The third section (Figure 16c) is a projection on the ECORS-CROP profile of the focal solutions computed in the northern part of the Briançonnais zone (to the north of the studied area) close to the profile after *Sue et al.* [1999]. In this sector, the belt is quite cylindrical. At the scale of the ECORS-CROP profile, i.e., of the alpine crust as a whole, the control of the extension by the CPF geometry is clear. The CPF is reactivated as a crustal extensional detachment, as most normal focal solutions are projected on the reflectors associated to this former thrust. Thus, at every scale and using both structural geology and seismology, we found the same kind of relationships between the extensional tectonic regime and the CPF, which represent the major inherited crustal discontinuity in this region.

[26] To sum up, our multidisciplinary approach allows us to point out several active faults in the Briançon-Guillette region, mainly belonging to the longitudinal family. Nevertheless, the transverse family may also control part of the present-day regional seismic activity. This suggests that the whole fault network studied in the field is still active and controls the present-day tectonic activity of the region. One of the major results raised by the combination of the complementary seismotectonic and structural approaches is the coherency and continuity we established between the late alpine and the current extensional tectonics in the southwestern internal Alps.

5. Neogene to Current Tectonics in the Western Alps: An Attempt at Synthesis

[27] Several methods have been used in the Alps to analyze the recent and current tectonics of the belt: fault analyses, fission track, seismology, geodesy, etc. A global view of the Neogene to current alpine tectonics must take those various and complementary methods into account. This synthesis is shown on Figure 17.

5.1. Brittle Tectonics

[28] To the east the brittle extension affected the Piemonte zone up to the Viso ophiolitic massif [*Lazarre et al.*, 1994; *Schwartz*, 2002]. In the Viso massif region the brittle extension is linked and preceded by a ductile extension (see section 2), which allowed the exhumation of the high-

pressure/high-temperature units of Mont Viso and Dora Maira massifs [*Schwartz*, 2002].

[29] To the north the inversion of the CPF as a normal fault has been proposed by *Aillères et al.* [1995], who showed that a Neogene extension affected the “Briançonnais Zone Houillère,” and *Cannic et al.* [1999], who pointed out a ductile extension in the Valais units between the CPF and the Briançonnais front. More to the north, using fission tracks, *Seward and Mancktelow* [1994] and *Fügenschuh et al.* [1999] established that a Neogene extension could have affected the SE side of the Mont Blanc external crystalline massif and the internal zones. This extension is associated to the uplift of the Mont Blanc massif [*Levallois*, 1972; *Schaer and Jeanrichard*, 1974; *Fourniguet*, 1977]. In the Val d’Aosta area, *Bistacchi et al.* [2000, 2001] also found extensional faulting with a stretching direction parallel to the belt, and they proposed an extrusion of this area toward the SW. At the eastern tip of the internal penninic zones, *Mancktelow* [1985, 1992] described the extension along the Simplon fault zone (downthrow to the south), also affected by transcurrent dextral motions [*Burkhard*, 1986; *Hubbard and Mancktelow*, 1992].

[30] To the south of the western Alps, mainly in the external zone, *Labauve et al.* [1989] have found two faulting events posterior to the Miocene alpine shortening. They described normal faults with an E-W extension to the northwest and eastern sides of the Argentera external crystalline massif. Strike-slip reactivation would have affected the normal faults during the Quaternary, with dextral motions along the longitudinal faults: Here, the transcurrent tectonic regime becomes dominant (e.g., Bersezio fault, to the south of the Serenne fault). Westward to the outer zone of the belt, they found a compression perpendicular to the alpine front.

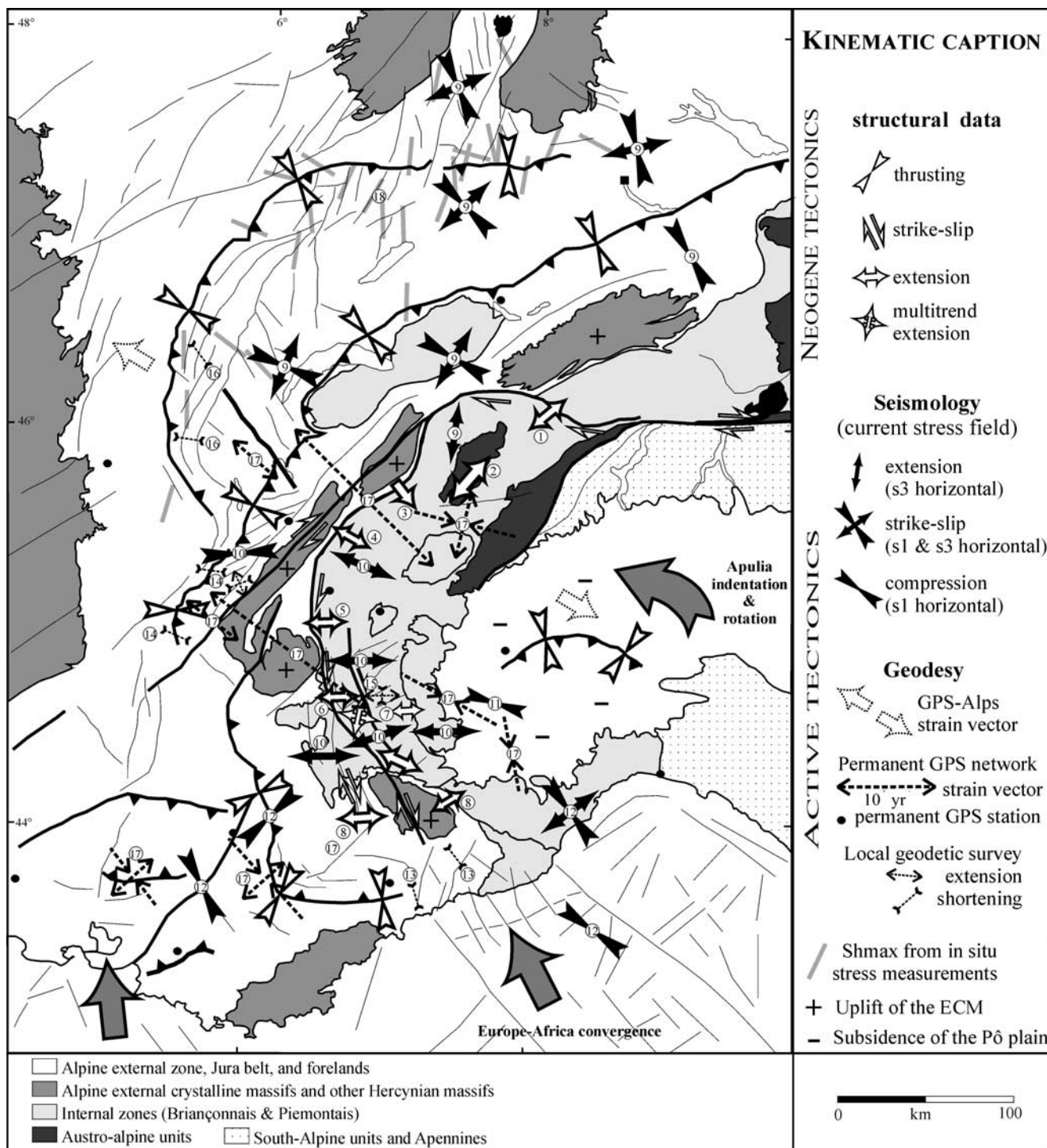
[31] To the west, in the external zone, the Neogene tectonics is marked by thrusting at the front of the alpine arc [*Grellet et al.*, 1993], propagation of crustal thrust ramp at the front of the external crystalline massifs and associated with their uplift, and dextral transcurrent motions longitudinal to the belt [*Ménard*, 1988], probably with conjugate sinistral strike-slip motions radial to the belt [*Thouvenot et al.*, 1998]. Thrusts propagate radially to the outermost zone of the belt (Plio-Quaternary deformation map of *Grellet et al.* [1993]). Nevertheless, indications of active thrusting to the front of the belt remain scarce (see below). Particularly, in the Jura belt, to the northwestern tip of the alpine belt, the

Figure 16. (opposite) Three imbricated multiscale cross sections, perpendicular to the belt’s trend (see insert for location). Their comparison establishes the close relationships between late alpine and active faulting. Actually, the same basic extensional tectonic features are found: (a) on the field (Oreac cross section [*Sue and Tricart*, 1999]); (b) at the upper crustal scale with a seismotectonic cross section across the Durance Valley (CS4, see Figure 14 for precise location); (c) at the ECORS-CROP profile scale [after *Sue et al.*, 1999, Figure 4]. The distance from this cross section to the ECORS profile ranges from 10 to 20 km, which justifies the projection in this part of the belt locally quite cylindrical. Extension develops at every scale, and the normal faults such as the Durance fault are clearly still active (see also Figure 14 and 15). Moreover, the CPF has a major role in this extension as it localizes the base of the normal faults. Actually, the CPF works as a basal detachment with respect to the Neogene to current extensional regime, at least in the studied area. Note that the three cross sections do not lay on the same transverse. Thus the boxes only give the equivalent position of the corresponding cross section.

main frontal thrust would be inactive since 5 Ma, and only the southern Jura would be still thrusting [Jouanne *et al.*, 1998; Becker, 2000]. In this tectonic framework the Plio-Quaternary tectonics of the outer arc of the western Alps may work in the continuity of the Miocene compressive radial tectonic regime.

[32] Extensional tectonics has been described in several areas of the internal western Alps. The whole internal zones,

from the Simplon fault to the back of the Argentera massif, have undergone such extensional tectonics at least during part of the Neogene. The CPF appears to have a major role in the development of this extensional tectonic regime in the internal zones, which worked coevally with the propagation of the alpine front toward the outermost zones of the belt and the foreland. Figure 17 presents a synthesis of the Neogene tectonics in the belt (white arrows). The counter-



clockwise rotation of the Apulo-Adriatic indenter may account for the dextral transcurrent motions developed all along the western and central alpine belt parallel to its trend [Ménard, 1988; Vialon *et al.*, 1989; Thomas *et al.*, 1999; Collombet *et al.*, 2002]. At several places, these large dextral faults crossed the CPF and died out in the external zone (e.g., the Belledonne, Parpaillon, and Argentera faults).

5.2. Seismicity

[33] The widespread Neogene extensional tectonic regime of the internal zones of the belt is closely associated with the widespread seismic extension established by Sue *et al.* [1999]. This synthesis is aimed to specify the relationship between the western European, the external alpine, and the internal alpine stress fields (Figure 17).

[34] The western European stress field is characterized by a NW-SE direction for the maximum stress due to the converging European and African plates and to the pushing of the North Atlantic mid-oceanic ridge [Zoback *et al.*, 1989; Zoback, 1992; Müller *et al.*, 1992; Grünthal and Stromeyer, 1992; Rebai *et al.*, 1992]. The mean direction varies from NNW-SSE to NW-SE [Müller *et al.*, 1992] but overall remains quite stable, except in the vicinity of the alpine belts (Alps, Pyrénées, Apennines). In particular, because of their arcuate geometry the western Alps are an important perturbation within the far-field west European stress field [Müller *et al.*, 1992; Rebai *et al.*, 1992; Philip, 1987].

[35] The external western Alps stress field presents globally a radial shape for the maximal stress axis inferred from earthquake focal mechanisms at the scale of the arc as a whole [e.g., Pavoni, 1986]. The northern part of the western Alps, the Jura, the southern side of the Rhine graben, show a NW-SE maximal stress direction comparable to the western European stress. The earthquake-related data are quite numerous in the external western Alps: P axes focal solutions [Ahorner *et al.*, 1972; Pavoni, 1980; Nicolas *et al.*, 1990; Roth *et al.*, 1992; Delouis *et al.*, 1993;

Maurer and Deichmann, 1995; Baer *et al.*, 1997; Eva *et al.*, 1997; Maurer *et al.*, 1997; Pavoni *et al.*, 1997; Eva *et al.*, 1998] and focal solution inversions [Carey-Gaihardis and Mercier, 1992; Plenefisch and Bonjer, 1997; Sue *et al.*, 1999; Baroux *et al.*, 2001; U. Kastrup *et al.*, Stress field variations in the Swiss Alps and the northern Alpine foreland derived from inversion of fault plane solutions, submitted to *Journal of Geophysical Research*, 2003, hereinafter referred to as Kastrup *et al.*, submitted manuscript, 2003]. In the Jura belt, where very few focal solutions are available, in situ stress measurements exhibit mainly N-S direction of S_{hmax} [Becker *et al.*, 1987; Becker, 1989; Becker and Werner, 1995; Becker, 1999, 2000]. In this area, it seems that the current state of stress is not affected by the alpine dynamics, as it is fairly far from radial compression. There would be a discrepancy between the focal-solution-related stress field in the alpine realm and the in situ stress measurements in the Jura belt, which can be explained by the distance between the alpine orogen's core and the Jura. Nevertheless, using focal solutions in the outer arc of the western Alps, from the Préalps to the Pelvoux massif, the external alpine stress field appears to be dominated by a compression radial to the arc [Ahorner *et al.*, 1972; Fréchet, 1978; Pavoni, 1986; Ménard, 1988; Müller *et al.*, 1992]. The maximal stress would be deviated from the global European direction by the Apulo-Adriatic indenter [Pavoni, 1961; Tapponnier, 1977]. The focal solutions available from the southern tip of the western external Alps to the Ligurian sea show P axes directions from NW-SE to E-W compatible with the radial compression to the front of the belt and with the Europe-Africa convergence across the western Mediterranean area [Bethoux *et al.*, 1988, 1992; Baroux *et al.*, 2001]. Note that these maximal horizontal stress directions are often associated with strike slip in terms of deformation. Globally, the current stress field S_{hmax} in the external zone of the western Alps (front of the belt) and in the near foreland is radial to the trend of the belt and associated with transcurrent/transpressive deformation style.

[36] The internal western Alps stress field is characterized by a radial extension at the scale of the belt [Sue *et al.*,

Figure 17. (opposite) Neogene to ongoing tectonics in the western Alps: a geographical, temporal, and methodological synthesis. Neogene tectonics is symbolized by the white arrows. In the external zone, westward propagation of the front of the belt (thrusting) is the dominant tectonic feature [Grellet *et al.*, 1993]. In the whole internal zones, extensional tectonics is clearly dominant. Note the dextral strike-slip longitudinal to the belt [e.g., Ménard, 1988]. Current stress field inferred from inversion of focal solutions is symbolized by black arrows. The external zone and foreland are characterized by transcurrent to compressive stress fields, with S_{hmax} radial to the belt, except in the Jura, where in situ measurements exhibit N-S directed S_{hmax} . On the contrary, the inner western Alps are characterized by a widespread extension radial to the belt. The active strains measured using geodetic methods are represented by dotted symbols: the bold dotted arrows represent the strain tensors obtained using the permanent GPS stations in vicinity of the western Alps [Calais *et al.*, 2002]. The two largest dotted arrows represent the GPS-Alps mean strain vector [Vigny *et al.*, 2002]. Other local geodetic surveys are also shown by the small dotted symbols. The complex alpine tectonic framework may emerge from interactions between forces at the limits of the belt (alpine collision, block kinematics) and buoyancy forces in the root of the belt. Reference indexes plotted inside small circles on the map are (1) Mancktelow [1992]; (2) Bistacchi *et al.* [2001]; (3) Seward and Mancktelow [1994]; (4) Cannic *et al.* [1999]; (5) Aillères *et al.* [1995]; (6) Sue and Tricart [1999]; (7) Schwartz *et al.* [2003]; (8) Labaume *et al.* [1989]; (9) Kastrup *et al.* (submitted manuscript, 2003); (10) Sue *et al.* [1999]; (11) Eva *et al.* [1997]; (12) Baroux *et al.* [2001]; (13) Calais *et al.* [2000]; (14) Martinod *et al.* [1996]; (15) Sue *et al.* [2000]; (16) Jouanne *et al.* [1998]; (17) Calais *et al.* [2002]; and (18) Becker [2000].

1999, Kastrup et al., submitted manuscript, 2003]. This is a major perturbation of the global European and alpine stress fields. The extensional stress field develops up to the northern tip of the internal western Alps [Maurer et al., 1997; Eva et al., 1998; Kastrup et al., submitted manuscript, 2003]. In the northwestern Alps this extensional stress field seems to coincide with the penninic nappes, especially in the Briançon area [Sue et al., 2003]. In the southwestern Alps it seems to end at the tip of Penninic nappes, where the CPF meets the Ivrea body [Paul et al., 2001; Bethoux et al., 2003]. The eastern boundary of the extension could be associated to the western side of the Ivrea body and/or the insubric line. The western boundary could be marked by the CPF in a first approximation, except in the basement between the Pelvoux and Argentera massifs, and other local areas of the external crystalline massifs. Actually, the western boundary could be the basement culmination line (structure of Ménard [1979]) of the external crystalline massifs. A synthetic view of the western alpine current stress field is given Figure 17 (black arrows).

5.3. Geodesy

[37] In terms of vertical motions, accurate data are only available for the Swiss Alps, where uplift rates reach up to 1.4–1.6 mm/yr in the Valais and High Grison areas [Gubler et al., 1981]. In term of horizontal displacements, there have been several recent geodetic campaigns in the western Alps, using comparison between triangulation and GPS measurements. All these geodetic surveys found small strain rates and deformation velocities [e.g., Calais, 1999]. Local surveys often qualitatively agreed with known tectonic and seismotectonic features of the area. In the outer part of the southwestern Alps, Jouanne et al. [2001] have proposed very moderate deformations in the Digne nappe and the northern Valensole basin, compatible with shortening at the front of the nappe and with still active thrusting. In the Grenoble-Belledonne area, Martinod et al. [1996] found mainly strike-slip motion between Belledonne external crystalline massif and the subalpine massifs (Chartreuse, Vercor), in good agreement with the local seismicity [Thouvenot, 1996]. Jouanne et al. [1998] also pointed out qualitatively such transcurrent deformation associated with thrusting in front of the subalpine Jura chain (deformation rate in the range of 3–4 mm/yr). In the southwestern Alps, Calais et al. [2000] established a NW-SE to N-S compressive strain, which is also in good agreement with the local seismicity (deformation rate in the range of 2–4 mm/yr). In the Briançon region (internal zone), Sue et al. [2000] found locally extensive deformation (E-W extension of about 2–4 mm/yr) exactly at the place of intensive extensional seismicity (see section 4), showing a remarkable agreement between geological, seismological, and geodetic approaches. Moreover, the reiteration of the GPS-Alps (a temporary GPS network of 60 sites in the western Alps) measurements (first measured in 1993, remeasured in 1998) has recently shown the same kind of extensional strain across the western Alps as a whole [see Vigny et al., 2002, Figure 5 insert]. Another large-scale geodetic

survey by Calais et al. [2002] has recently confirmed the main part of extensional strain in the western Alps using 6 years of continuous geodetic measurements across the whole belt (1 mm/yr of E-W extension in the central western Alps, 1 mm/yr of N-S shortening in the southwestern Alps). Thus three independent geodetic surveys have recovered the extensional active tectonics in the inner western Alps. These result strengthen the seismotectonic and structural approaches: Independent structural and geophysical methods provided coherent results showing recent and still active extensional tectonics in the western Alps.

6. Discussion

[38] We characterized the tectonic evolution of a central area in the internal western Alps using a multidisciplinary approach. This area, in the core of the alpine arc, allows better understanding of the neotectonic evolution of the belt. An extensional tectonic regime developed here during the Neogene. Extensional tectonics has been shown first to develop in the internal zones of the western Alps and second to also rule their present-day tectonics. This part of the alpine evolution must now be considered as an important aspect of the dynamics of the belt. The now well-established extensional tectonics has such geographical widespread and temporal duration that it should be invoked as an important part of alpine geodynamics. Several independent methods all provided coherent results, including brittle deformation analysis, seismotectonics, strain measurement (geodesy), and paleostress and current stress fields. They allow the proposal of an overall continuity of (1) Neogene tectonics with the development of normal faults and related extensional structures and (2) present-day tectonics dominated by a moderate seismicity due to generalized extension in the internal zones of the belt. Part of the deformation observed in the internal western Alps is also associated with transcurrent motions. Strike slip also affects the external zone, where the overall stress field seems to be transpressive. To the north, normal faulting is also often associated with transcurrent motions (e.g., Simplon area). Although extensional tectonics appears as the major tectonic feature of the internal western Alps, we can propose that the state of stress in the internal zone, which controls the extensional tectonics, was actually metastable and may switch from an extensional state to a more transcurrent state. This instability could emerge from interferences between driving forces for the extension and counterclockwise rotational phenomenon in the western Alps [Gidon et al., 1964; Anderson and Jackson, 1987; Ménard, 1988; Vialon et al., 1989; Thomas et al., 1999; Collombet et al., 2002].

[39] Beyond the data analysis, our results raise up major issues in term of geodynamic interpretations. The discussion about the driving forces for the extensional tectonics in the Alps remains lively, and we still need additional data strengthened by modeling to increase our understanding. Nevertheless, several hypotheses can be advanced. Basically, three classes of dynamic models can be proposed:

(1) complex block-kinematic related extension, (2) shallow extension above an ascending deep indenter, and (3) buoyancy forces related extension.

[40] 1. Block-kinematic models tend to explain the late alpine extensional tectonics by transtension due to lateral motions of homogeneous blocks in the belt in response to Adria indentation [Bistacchi *et al.*, 2000]. Such extrusion tectonics, observed in the eastern Alps [Ratschbacher *et al.*, 1991], a priori lacks a free boundary in the western Alps. An alternative model would be block rotation in the belt in response to Adria counterclockwise rotation [e.g., Collombet *et al.*, 2002], in which the rotation may induce the extensional tectonics in the core of the belt [Calais *et al.*, 2002]. A major issue is that such models (lateral escape or rotation) imply orogen-parallel extension, whereas radial extension is observed in the western Alps through the seismotectonic analysis.

[41] 2. Shallow extension above a deep indenter has been proposed by Schwartz *et al.* [1999] to explain the ductile then brittle extension, as well as the exhumation of high-pressure rocks in the Piemontais zone. This model, which depends on the deep structures of the belt [e.g., Kissling, 1993; Paul *et al.*, 2001], would imply deep compressional tectonics and overall shortening across the belt as a whole, which is not still documented.

[42] 3. Buoyancy force related extension may be observed in several geodynamic contexts that may correspond at least partly to the western Alps: the collapse of an overthickened crust [Molnar and Lyon-Caen, 1988], although the depth of the alpine crustal roots remains moderate [Waldhauser *et al.*, 1998]; a slab break off [Blanckenburg and Davies, 1995], implying rapid uplift and heating, which are not observed in the Alps; and a back-arc-like extension driven by subduction retreat [Royden, 1993]. This last model meets the thermomechanical model of Burov *et al.* [1999] and could explain the decoupling between external and internal alpine arcs, but it

implies adaptation of active margin dynamics to a collision belt.

7. Conclusion

[43] To characterize the late alpine (i.e., Neogene) to present-day tectonics in a key area of the southwestern Alps, we used a combined approach with fault analyses using structural geology and seismotectonics. We established a complex tectonic regime, dominated by extension but also showing strike-slip motions. Good coherency of the brittle deformation observed on the field (Neogene tectonics) with the seismotectonic observations (active tectonics) has been established, which suggests a tectonic continuity from the Neogene onward. This still active extensional tectonics is characteristic for the Briançonnais-Ubaye-Queyras area and developed in the whole internal zones of the belt. Because of its widespread geographical distribution and temporal duration this extensional phase appears now as a major evolution of the alpine tectonics. Nevertheless, it raises important issues about geodynamic models. The complex tectonic framework of the alpine collision between European plate and Adria indenter (block-kinematics, deep indenter), possibly associated with buoyancy forces in the root of the belt, may explain the observed Neogene to current extensional tectonics in the core of the Alps.

[44] **Acknowledgments.** This work was supported by the Neuchâtel and Grenoble (UJF) Universities, by the Swiss National Science Foundation (grant 21-61684-00), by the French CNRS, and by the French Program GéoFrance3D (contribution 122). We thank F. Roue, A. W. Bally, and an anonymous reviewer for their very constructive reviews. Many thanks to M. Burkhard, J. D. Champagnac, B. Delacou, A. Pfiffner, and M. E. Claudel for fruitful discussions and comments and to Ombeline for her support. We are grateful to G. Vidal for his work on the DEM, to the Sismalp group for making their data available, and to T. Villemin for providing his stress software. We wish to thank K. Verrecchia for many improvements in the English language. Maps were drawn using the GMT software [Wessel and Smith, 1991].

References

- Ahorer, Z., H. Murawski, and G. Scheinder, Sismo-tektonische Traverse von der Nordsee bis zum Apennin, *Geol. Rundsch.*, 61, 915–942, 1972.
- Aillères, L., J. M. Bertrand, and M. Champenois, New structural data from the “Zone Houillère Briançonnaise” (French Alps), nealpine Tectonics and consequences for the interpretation of the Pennine Front, *C. R. Acad. Sci.*, 321, 247–254, 1995.
- Amelung, F., and G. King, Large-scale tectonic deformation inferred from small earthquakes, *Nature*, 386, 702–705, 1997.
- Anderson, H., and J. Jackson, Active tectonics in the Adriatic region, *Geophys. J. R. Astron. Soc.*, 91, 937–983, 1987.
- Angelier, J., Sur l’analyse de mesures recueillies dans les sites faillés: L’utilité d’une confrontation entre les méthodes dynamiques et cinématiques, *C. R. Acad. Sci.*, 281, 1805–1808, 1975.
- Angelier, J., Tectonic analysis of fault slip data sets, *J. Geophys. Res.*, 89, 5835–5848, 1984.
- Angelier, J., From orientation to magnitudes in paleo-stress determinations using fault slip data, *J. Struct. Geol.*, 11, 37–50, 1989.
- Angelier, J., Inversion of field data in fault tectonics to obtain the regional stress—A new rapid direct inversion method by analytical means, *Geophys. J. Int.*, 103, 363–376, 1990.
- Angelier, J., and J. Goguel, Sur une méthode simple de détermination des axes principaux des contraintes pour une population de failles, *C. R. Acad. Sci.*, 282, 307–310, 1979.
- Angelier, J., and P. Mechler, Sur une méthode graphique de recherche des contraintes principales également utilisable en tectonique et Séismologie: La méthode des dièdres droits, *Bull. Soc. Géol. Fr.*, 7(19), 1309–1318, 1977.
- Argand, E., La tectonique de l’Asie, *Proc. Int. Geol. Congr.*, 1, 171–372, 1924.
- Baer, M., N. Deichmann, D. Fäh, U. Kradolfer, D. Mayer-Rosa, E. Rüttener, T. Schler, S. Sellami, and P. Smit, Earthquakes in Switzerland and surrounding regions during 1996, *Eclogae Geol. Helv.*, 90, 557–567, 1997.
- Ballevre, M., Y. Lagabrielle, and O. Merle, Tertiary ductile normal faulting as a consequence of lithospheric stacking in the western Alps, *Mém. Soc. Géol. Fr.*, 156, 227–236, 1990.
- Barféty, J.-C., Lemoine, D. Mercier, R. Polino, P. Nievergelt, J. Bertrand, T. Dumont, S. Amaudric du Chaffaut, A. Pêcher, and G. Montjuvent, Geological map of France, scale 1/50,000, feuille Briançon, Bur. De Rech. Geol. et Minere, Orléans, France, 1996.
- Baroux, E., N. Béthoux, and O. Bellier, Analyses of the stress field in southeastern France from earthquake focal mechanisms, *Geophys. J. Int.*, 145, 336–348, 2001.
- Becker, A., Detached neotectonics stress field in the northern Jura Mountains, Switzerland, *Geol. Rundsch.*, 78, 459–475, 1989.
- Becker, A., In situ stress data from the Jura Mountains—New results and interpretation, *Terra Nova*, 11, 9–15, 1999.
- Becker, A., The Jura Mountains—An active foreland fold-and-thrust belt?, *Tectonophysics*, 312, 318–406, 2000.
- Becker, A., and D. Werner, Neotectonic state of stress in the Jura Mountains, *Geodyn. Acta*, 8(2), 99–111, 1995.
- Becker, A., P. Blüming, and W. H. Müller, Recent stress field and neotectonics in the eastern Jura mountains, Switzerland, *Tectonophysics*, 135, 277–288, 1987.
- Béthoux, N., M. Cattaneo, P. Y. Delpéch, C. Eva, and J.-P. Réhault, Mécanismes au foyer de séismes en mer Ligure et dans le sud des Alpes occidentales:

- Résultats et interpretation, *C. R. Acad. Sci.*, 307, 71–77, 1988.
- Béthoux, N., J. Fréchet, F. Guyotot, F. Thouvenot, M. Cattaneo, C. Eva, M. Nicolas, and M. Granet, A closing Ligurian Sea?, *Pure Appl. Geophys.*, 139, 179–194, 1992.
- Béthoux, N., C. Sue, A. Paul, J. Virieux, M. Cattaneo, J. Fréchet, and F. Thouvenot, Local tomography and focal mechanisms in the western Alps: Comparison of methods: Tectonic implications, *Tectonophysics*, in press, 2003.
- Bistacchi, A., E. Eva, M. Massironi, and S. Solarino, Miocene to present kinematics of the NW-Alps: Evidence from remote sensing, structural analysis, seismotectonics and thermochronology, *J. Geodyn.*, 30, 205–228, 2000.
- Bistacchi, A., G. V. Dal Piaz, M. Massironi, M. Zattin, and M. L. Balestrieri, The Aosta-Ranzola extensional fault system and Oligocene-Present evolution of the Austroalpine-Penninic wedge in the north-western Alps, *Int. J. Earth. Sci.*, 90, 654–667, 2001.
- Black, M. C., and A. Jayko, Uplift of very high pressure rocks in the western Alps: Evidence for structural attenuation along low angle faults, in *Deep Structure of the Alps*, edited by F. Roure, P. Heitzmann, and R. Polino, *Mem. Soc. Géol. Fr.*, 156, 228–237, 1990.
- Blanckenburg, F. von, and J. H. Davies, Slab breakoff: A model for synconglomeratic magmatism and tectonics in the Alps, *Tectonics*, 14, 120–131, 1995.
- Bott, M. H., The mechanism of oblique slip faulting, *Geol. Mag.*, 96(2), 109–117, 1959.
- Burkhard, M., Déformation des calcaires de l'Helvétique de la Suisse occidentale (Phénomènes, mécanismes et interprétations tectoniques), *Rev. Géol. Dyn. Géogr. Phys.*, 27(5), 281–301, 1986.
- Burov, E., Y. Podladchikov, G. Grandjean, and J.-P. Burg, Thermo-mechanical approach to validation of deep crustal and lithospheric structures inferred from multidisciplinary data: Application to the western and northern Alps, *Terra Nova*, 11, 124–131, 1999.
- Calais, E., Crustal deformation in the western Alps from continuous GPS measurements, 1996–1998, *Geophys. J. Int.*, 38, 221–230, 1999.
- Calais, E., L. Galissot, J.-F. Stéphan, J. Delteil, J. Deverchère, C. Larroque, B. Mercier de Lépinay, M. Popoff, and M. Sosson, Crustal strain in the southern Alps, 1948–1998, *Tectonophysics*, 319, 1–17, 2000.
- Calais, E., J. M. Nocquet, F. Jouanne, and M. Tardy, Current strain regime in the western Alps from continuous Global Positioning System measurements, 1996–2001, *Geology*, 30, 651–654, 2002.
- Cannic, S., J.-L. Mugnier, and J.-M. Lardeaux, Neogene extension in the western Alps, *Mem. Sci. Geol. Padova*, 51(1), 33–45, 1999.
- Carey, E., and B. Brunier, Analyse théorique et numérique d'un modèle mécanique élémentaire appliqué à l'étude d'une population de failles, *C. R. Acad. Sci.*, 279, 891–894, 1974.
- Carey-Gaihardis, E., and J.-L. Mercier, Regional state of stress, fault kinematics and adjustments of blocks in a fractured body of rock: Application to the microseismicity of the Rhine graben, *J. Struct. Geol.*, 14, 1007–1017, 1992.
- Channel, J. E. T., B. D'Argenio, and F. Horvath, Adria, the African promontory in Mesozoic Mediterranean paleogeography, *Earth Sci. Rev.*, 15, 213–292, 1979.
- Claudel, M. E., and T. Dumont, Early and late Jurassic rifting events in the French Briançonnais relative to the evolution of the Ligurian Tethys and Valais oceans, *Eclogae Geol. Helv.*, 92, 45–61, 1999.
- Collombet, M., J. C. Thomas, Y. Chauvin, P. Tricart, J. P. Bouillin, and J. P. Gratier, Counterclockwise rotation of the western Alps since the Oligocene: New insights from paleomagnetic data, *Tectonics*, 21(4), 1032, doi:10.1029/2001TC901016, 2002.
- Coward, M. P., D. Dietrich, and R. G. Park (Eds.), *Alpine Tectonics*, *Geol. Soc. Spec. Publ.*, 45, 1989.
- Debelmas, J., and M. Lemoine, Carte géologie France, scale 1/50, 000, feuille Guillestre, Bur. de Rech. Geol. et Minère, Orléans, France, 1966.
- de Graciansky, P.-C., G. Dardeau, M. Lemoine, and P. Tricart, The inverted margin in the French Alps and foreland basin inversion, in *Inversion Tectonics*, edited by M. A. Cooper and G. D. Williams, *Geol. Soc. Spec. Publ.*, 44, 87–104, 1989.
- Delouis, B., H. Haessler, A. Cisternas, and L. Rivera, Stress tensor determination in France and neighbouring regions, *Tectonophysics*, 10, 49–68, 1993.
- Dewey, J. F., M. L. Helman, E. Turco, D. W. H. Hutton, and S. D. Knott, Kinematics of the western Mediterranean, in *Alpine Tectonics*, edited by M. P. Coward, D. Dietrich, and R. G. Park, *Geol. Soc. Spec. Publ.*, 45, 265–283, 1989.
- Etchecopar, A., G. Vasseur, and M. Daignières, An inverse problem in microtectonics for the determination of stress tensor from fault striation analysis, *J. Struct. Geol.*, 3, 51–65, 1981.
- Eva, E., S. Solarino, C. Eva, and G. Neri, Stress tensor orientation derived from fault plane solution in the southwestern Alps, *J. Geophys. Res.*, 102, 8171–8185, 1997.
- Eva, E., S. Pastore, and N. Deichmann, Evidence for ongoing extensional deformation in the western Swiss Alps and thrust-faulting in the southwestern Alpine foreland, *J. Geodyn.*, 1, 27–43, 1998.
- Fourniguet, J., Mise en évidence de mouvements néotectoniques actuels verticaux dans le Sud-Est de la France par comparaison de nivellements successifs, *Rap. BRGM 77SGN081GEO*, pp. 1–35, Bur. des Rech. Geol. et Minère, Orléans, France, 1977.
- Fréchet, J., Sismicité du sud-est de la France et une nouvelle méthode de zonage sismique, thesis, Univ. Sci. Technol. Med., Grenoble, France, 1978.
- Frey, N., J. Desmons, and F. Neubauer, Metamorphic maps of the Alps, *Schweiz. Mineral. Petrogr.*, 79, 1999.
- Fügenschuh, B., A. Loprieno, S. Ceriani, and S. Schmid, Structural analysis of the Subbriançonnais and Valais units in the area of Moûtiers (Savoie, western Alps): Paleogeographic and tectonic consequences, *Int. J. Earth Sci.*, 88, 201–218, 1999.
- Gidon, M., C. Kerckhove, A. Michard, P. Tricart, and B. Goffé, Carte géologie France, scale 1/50, 000, feuille Aiguille de Chambeyron, Bur. de Rech. Geol. et Minère, Orléans, France, 1994.
- Gratier, J.-P., G. Ménard, and R. Arpin, Strain-displacement compatibility and restoration of the Châinnes Subalpines of the western Alps, in *Alpine Tectonics*, edited by M. P. Coward, D. Dietrich, and R. G. Park, *Geol. Soc. Spec. Publ.*, 45, 65–81, 1989.
- Grellet, B., P. Combes, T. Granier, and H. Philip, Sismotectonique de la France métropolitaine dans son cadre géologique et géophysique, *Mém. Soc. Géol. Fr.*, 164, 75 pp., 1993.
- Grünthal, G., and D. Stromeyer, The recent stress field in central Europe: Trajectories and finite element modeling, *J. Geophys. Res.*, 97, 1803–1805, 1992.
- Gubler, E., H. G. Kahle, E. Klinge, S. Mueller, and R. Olivier, Recent crustal movements in Switzerland and their geophysical interpretation, *Tectonophysics*, 71, 125–152, 1981.
- Hubbard, M., and N. S. Mancktelow, Lateral displacement during Neogene convergence in the western and central Alps, *Geology*, 20, 943–946, 1992.
- Jouanne, F., N. Genaudeau, G. Menard, and X. Darmendrail, Estimating present-day displacement fields and tectonic deformation in active mountain belts: an example from the Chartreuse Massif and the southern Jura Mountains, western Alps, *Tectonophysics*, 296, 403–419, 1998.
- Jouanne, F., J. C. Hippolyte, J. F. Gamond, and J. Martinod, Current deformation of the Digne Nappe (southwestern Alps) from a comparison between triangulation and GPS data, *Geophys. J. Int.*, 144, 432–440, 2001.
- Kerckhove, C., et al., Carte géologie France, scale 1/250, 000, feuille Gap, Bur. de Rech. Geol. et Minère, Orléans, France, 1979.
- Kissling, E., Deep structure of the Alps: What do we really know?, *Phys. Earth Planet. Inter.*, 79, 87–112, 1993.
- Labaume, P., J. F. Ritz, and H. Philip, Failles normales récentes dans les Alpes sud-occidentales: Leurs relations avec la tectonique compressive, *C. R. Acad. Sci.*, 308, 1553–1560, 1989.
- Laubscher, H., The arc of the western Alps today, *Eclogae Geol. Helv.*, 84, 631–659, 1991.
- Lazare, J., P. Tricart, and T. Villemin, L'extension cassante tardi-orogénique dans les schistes lustrés piémontais du Queyras (Alpes occidentales, France), *C. R. Acad. Sci.*, 319, 1415–1421, 1994.
- Lee, W. H., and J. E. Lahr, HYPO71: A computer program for determining hypocenter, magnitude and first-motion pattern of local earthquakes, *U.S. Geol. Surv. Open File Rep.*, 75–331, 1975.
- Lemoine, M., and P. Tricart, From oceanic closure to continental collision; a synthesis of the "schistes lustrés" metamorphic complex of the western Alps: Alternative interpretation, *Geol. Soc. Am. Bull.*, 105, 845–847, 1993.
- Lemoine, M., et al., The continental margin of the Mesozoic Tethys in the western Alps, *Mar. Pet. Geol.*, 3, 179–199, 1986.
- Levallois, J. J., Sur la mise en évidence d'un mouvement de surrection des massifs cristallins alpins, *Bull. Geod. Assoc. Int. Geod.*, 105, 299–312, 1972.
- Mancktelow, N., The Simplon line: A major displacement zone in the western Lepontine Alps, *Eclogae Geol. Helv.*, 78, 73–96, 1985.
- Mancktelow, N., Neogene lateral extension during convergence in the central Alps: Evidence from inter-related faulting and backfolding around the Simplon pass, Switzerland, *Tectonophysics*, 215, 295–317, 1992.
- Martinod, J., F. Jouanne, J. Tavera, G. Ménard, J. F. Gamond, X. Darmendrail, J. C. Notter, and C. Basile, Present-day deformation of the Dauphine (SE France) Alpine and Subalpine massifs, *Geophys. J. Int.*, 127, 189–200, 1996.
- Maurer, H., and N. Deichmann, Microearthquake cluster detection based on waveform similarities, with an application to the western Swiss Alps, *Geophys. J. Int.*, 123, 588–600, 1995.
- Maurer, H., M. Burkhard, N. Deichmann, and G. Green, Active tectonism in the central Alps: Contrasting stress regimes north and south of the Rhone Valley, *Terra Nova*, 9, 91–94, 1997.
- Ménard, G., Relations entre structures profondes et structures superficielles dans le Sud-Est de la France: Essai d'utilisation de données géophysiques, Thèse 3ème cycle, 178 pp., Univ. Grenoble, Grenoble, France, 1979.
- Ménard, G., Structure et cinématique d'une chaîne de collision: Les Alpes occidentales et centrales, thesis, Univ. J. Fourier, Grenoble, France, 1988.
- Molnar, P., and H. Lyon-Caen, Some simple physical aspects of the support, structure, and evolution of mountain belts, *Spec. Pap. Geol. Soc. Am.*, 218, 179–207, 1988.
- Mugnier, J.-L., H. Loubat, and S. Cannic, Correlation of seismic images and geology at the boundary between internal and external domains of the western Alps, *Bull. Soc. Géol. Fr.*, 164, 697–708, 1993.
- Müller, B., M. L. Zoback, K. Fuchs, S. Gregersen, N. Pavoni, O. Stephansson, and C. Ljunggren, Regional patterns of tectonic stress in Europe, *J. Geophys. Res.*, 97, 1783–1803, 1992.
- Nicolas, A., A. Hirn, R. Nicolich, R. Polino, and ECORS-CROP Working Group, Lithospheric wedging in the western Alps inferred from the ECORS-CROP traverse, *Geology*, 18, 587–590, 1990.
- Paul, A., M. Cattaneo, F. Thouvenot, D. Spallarossa, N. Béthoux, and J. Fréchet, A three-dimensional crustal structure velocity model of the southwestern Alps from local earthquake tomography, *J. Geophys. Res.*, 106, 19,367–19,389, 2001.
- Pavoni, N., Faltung durch horizontal verschiebung, *Eclogae Geol. Helv.*, 54, 515–534, 1961.
- Pavoni, N., Crustal stresses inferred from fault plane solutions of earthquakes and neotectonic deforma-

- tions in Switzerland, *Rock Mech.*, Suppl. 9, 63–68, 1980.
- Pavoni, N., Regularities in the pattern of major fault zones of the Earth and the origin of arcs, in *Origin of Arcs*, edited by F. C. Wezel, pp. 63–78, Elsevier Sci., New York, 1986.
- Pavoni, N., H. R. Maurer, P. Roth, and N. Deichmann, Seismicity and seismotectonics of the Swiss Alps, in *Deep Structure of the Swiss Alps: Results of NRP20*, edited by O. A. Pfiffner et al., pp. 241–250, Birkhäuser, Basel, Switzerland, 1997.
- Pécher, A., Schmidmac—A program to display and analyse directional data, *Comput. Geosci.*, 15(8), 1315–1326, 1989.
- Pfiffner, O. A., and M. Burkhard, Determination of paleo-stress axes orientations from fault, twin and earthquake data, *Ann. Tectonicae*, 1, 48–57, 1987.
- Philip, H., Plio-Quaternary evolution of the stress field in Mediterranean zones of subduction and collision, *Annls Geophys.*, 5, 301–320, 1987.
- Philippot, P., Opposite vergence of nappes and crustal extension in the French-Italian western Alps, *Tectonics*, 9, 1143–1165, 1990.
- Plenefisch, T., and K. P. Bonjer, The stress field in the Rhine Graben area inferred from earthquake focal mechanisms and estimation of frictional parameters, *Tectonophysics*, 275, 71–97, 1997.
- Ratschbacher, L., W. Frisch, H.-G. Linzer, and O. Merle, Lateral extrusion in the eastern Alps: 2. Structural analysis, *Tectonics*, 10, 257–271, 1991.
- Rebãi, S., H. Philip, and A. Taboada, Modern tectonic stress field in the Mediterranean region: Evidence for variation in stress directions at different scales, *Geophys. J. Int.*, 110, 106–140, 1992.
- Ritz, J.-F., Champ de contrainte dans les Alpes du Sud depuis 25 millions d'années. Implications géodynamiques et seismotectoniques, thèse, 187 pp., Univ. Montpellier, Montpellier, France, 1991.
- Ritz, J.-F., and A. Taboada, Revolution stress ellipsoids in brittle tectonics resulting from an uncritical use of inverse methods, *Bull. Soc. Géol. Fr.*, 164, 519–531, 1993.
- Roth, P., N. Pavoni, and N. Deichmann, Seismotectonics of the eastern Swiss Alps and evidence for precipitation-induced variations of seismic activity, *Tectonophysics*, 207, 83–97, 1992.
- Rothé, J. P., Les séismes des Alpes françaises en 1938 et la sismicité des Alpes occidentales, *Ann. Inst. Phys. Globe Strasbourg*, 3, 1–105, 1941.
- Royden, L. H., Evolution of retreating subduction boundaries formed during continental collision, *Tectonics*, 12, 629–638, 1993.
- Sassi, W., and E. Carey-Gailhardis, Interprétation mécanique du glissement sur les failles: Introduction d'un critère de frottement, *Ann. Tectonicae*, 2, 139–154, 1987.
- Schaer, J. P., and F. Jeanrichard, Mouvements verticaux anciens et actuels dans les Alpes suisses, *Eclogae Geol. Helv.*, 67, 101–119, 1974.
- Schmid, S., and E. Kissling, The arc of the western Alps in the light of geophysical data on deep structure, *Tectonics*, 19, 62–85, 2000.
- Schwartz, S., La zone piémontaise des Alpes occidentales: Un paléo-complexe de subduction. Arguments métamorphiques, géochronologiques et structuraux, *Doc. B.R.G.M.*, 302, 341 pp., 2002.
- Schwartz, S., J. M. Lardeau, A. Paul, M. Cattaneo, P. Tricart, S. Guillot, Y. Laggabrielle, and G. Poupeau, Syn-convergence extension, mantle indentation and exhumation of high-pressure rocks: Insights from the western Alps, *Abstract Suppl. EUG 10*, Eur. Union of Geophys., Strasbourg, France, 1999.
- Schwartz, S., J.-M. Lardeaux, G. Poupeau, P. Tricart, and E. Labrin, New apatite and zircon fission-tracks data in the Piémont zone of the western Alps: Tectonic consequences, *Tectonophysics*, in press, 2003.
- Seward, D., and N. Mancktelow, Neogene kinematics of the central and western Alps: Evidence from fission-track dating, *Geology*, 22, 803–806, 1994.
- Sue, C., Dynamique actuelle et récente des Alpes occidentales internes—Approche structurale et sismologique, thesis, Univ. J. Fourier, Grenoble, France, 1998.
- Sue, C., and P. Tricart, Late Alpine brittle extension above the Frontal Penninic Thrust near Briançon, western Alps, *Eclogae Geol. Helv.*, 92(2), 171–181, 1999.
- Sue, C., and P. Tricart, Late-Alpine syncollisional extension in the core of the western Alps inferred from faulting analysis, *J. Geol. Soc. London*, 159, 61–70, 2002.
- Sue, C., F. Thouvenot, J. Fréchet, and P. Tricart, Widespread extension in the core of the western Alps revealed by earthquake analysis, *J. Geophys. Res.*, 104, 25,611–25,622, 1999.
- Sue, C., J. Martinod, P. Tricart, F. Thouvenot, J. F. Gamond, J. Fréchet, D. Marinier, J.P. Glot, and J.R. Grasso, Active deformation in the inner western Alps inferred from comparison between 1972-classical and 1996-GPS geodetic surveys, *Tectonophysics*, 320, 17–29, 2000.
- Sue, C., J. R. Grasso, F. Lahaie, and D. Amitrano, Mechanical behavior of western alpine structures inferred from statistical analysis of seismicity, *Geophys. Res. Lett.*, 29(8), 1224, 10.1029/2001GL014050, 2002.
- Sue, C., P. Calcagno, G. Courrioux, P. Tricart, J. Fréchet, and F. Thouvenot, Relationship between inherited crustal structures and seismicity in the internal western Alps inferred from 3D modeling, *Tectonophysics*, in press, 2003.
- Tapponnier, P., Evolution tectonique du système alpin en Méditerranée: Poinçonnement et écrasement rigide-plastique, *Bull. Soc. Géol. Fr.*, 7, 437–460, 1977.
- Thomas, J. C., M. E. Claudel, M. Collombet, P. Tricart, A. Chauvin, and T. Dumont, First paleomagnetic data from the sedimentary cover of the French Penninic Alps: Evidence for Tertiary counterclockwise rotations in the western Alps, *Earth Planet. Sci. Lett.*, 171, 561–574, 1999.
- Thouvenot, F., Aspects géophysiques et structuraux des Alpes occidentales et de trois autres orogènes: Atlas, Pyrénées, Oural, thesis, Univ. J. Fourier, Grenoble, France, 1996.
- Thouvenot, F., et al., The M_L 5.3 Epagny (French Alps) earthquake of 1996 July 15: A long-awaited event on the Vuache Fault, *Geophys. J. Int.*, 135, 876–892, 1998.
- Tricart, P., From passive margin to continental collision: A tectonic scenario for the western Alps, *Am. J. Sci.*, 284, 97–120, 1984.
- Tricart, P., and M. Lemoine, From faulted blocks to megamullions and megaboudins: Tethyan heritage in the structure of the western Alps, *Tectonics*, 5, 95–118, 1986.
- Tricart, P., J. P. Bouillin, P. Dick, L. Moutier, and C. Xing, Le faisceau de failles de Haute-Durance et le rejeu distensif du front briannonnais au SE du Pelvoux (Alpes occidentales), *C. R. Acad. Sci.*, 323, 251–257, 1996.
- Tricart, P., S. Schwartz, C. Sue, G. Poupeau, and J. M. Lardeaux, La dénudation tectonique de la zone ultradauphinoise et l'inversion du Front Briançonnais au SE du Pelvoux (Alpes occidentales): Une dynamique miocène à actuelle, *Bul. Soc. Geol. Fr.*, 172, 49–58, 2001.
- Trumpy, R., Palaeotectonic evolution of the central and western Alps, *Geol. Soc. Am. Bull.*, 71, 843–908, 1960.
- Vialon, P., P. Rochette, and M. Ménard, Indentation and rotation in the western Alpine arc, in *Alpine Tectonics*, edited by M. P. Coward, D. Dietrich, and R. G. Park, *Geol. Soc. Spec. Publ.*, 45, 329–338, 1989.
- Vigny, C., et al., GPS network monitors the western Alps over a five year period: 1993–1998, *J. Geod.*, 76, 63–76, 2002.
- Virlovet, B., P. Tricart, and T. Villemin, Blocs basculés tardialpins dans les nappes briannonnaises de Haute-Durance (Alpes occidentales, France) et évolution néotectonique des zones internes, *C. R. Acad. Sci.*, 322, 475–481, 1996.
- Waldhauser, F., E. Kissling, J. Ansorge, and S. Müeller, 3D interface modelling with 2D seismic data: The Alpine crust-mantle boundary, *Geophys. J. Int.*, 135, 264–278, 1998.
- Wallace, R., Geometry of shearing stress and relation to faulting, *J. Geol.*, 59, 118–130, 1951.
- Wessel, P., and W. H. Smith, Free software helps map and display data, *Eos Trans. AGU*, 72, 441, 445–446, 1991.
- Zoback, M. L., First- and second-order patterns of stress in the lithosphere: The world stress map project, *J. Geophys. Res.*, 97, 1703–1728, 1992.
- Zoback, M. L., et al., Global patterns of tectonic stress, *Nature*, 341, 291–298, 1989.

C. Sue, Université de Neuchâtel, Institut de Géologie, Rue Argand, 11, CH-2007 Neuchâtel, Switzerland. (christian.sue@unine.ch)

P. Tricart, Laboratoire de Géodynamique des Chaînes Alpines, Observatoire des Sciences de l'Univers de Grenoble, BP53 - Bâtiment IRIGM, F-38041 Grenoble Cedex 9, France. (Pierre.Tricart@ujf-grenoble.fr)